

Article

Tourmalines as a Tool in Provenance Studies of Terrigenous Material in Extra-Carpathian Albian (Uppermost Lower Cretaceous) Sands of Miechów Synclinorium, Southern Poland

Jakub Kotowski , Krzysztof Nejbert and Danuta Olszewska-Nejbert

Faculty of Geology, University of Warsaw, Żwirki i Wigury 93, 02-089 Warszawa, Poland; knejbert@uw.edu.pl (K.N.); dolszews@uw.edu.pl (D.O.-N.)

* Correspondence: j.kotowski@uw.edu.pl

Received: 31 August 2020; Accepted: 14 October 2020; Published: 16 October 2020



Abstract: The mature transgressive Albian quartz sands in the Miechów Synclinorium contain a poor (<1%) heavy mineral suite consisting of tourmaline, rutile, garnet, staurolite, ilmenite, zircon, monazite, kyanite, and gahnite. The other minerals, especially those containing Fe and Ti (e.g., biotite), are subordinate. Over 512 tourmaline grains from seven outcrops in the Miechów Segment were analysed using electron probe microanalysis (EPMA). The majority of grains belong to the alkali tourmaline group in which the X-site is dominated by Na (0.4 to 0.9 apfu). Detrital tourmalines are mainly dravite with a prevalent schorl end-member with average X_{Mg} values over 0.6. Apart from Mg and Fe, the other Y-site cations rarely exceed 0.1 apfu. Fluorine content is usually below the detection limit. Their chemical composition suggests that most tourmaline grains were sourced from Al-rich and Al-poor metapelites/metapsammites. The main source rocks for the Albian sands were rocks from low- to medium-grade metamorphism, probably from Al-rich quartz-muscovite schist and/or muscovite rich gneisses. Additional minor source rocks were granites and pegmatites coexisting with them. A comparison of the examined tourmaline to tourmaline from possible source areas indicates that these areas were located in the eastern part of the Bohemian Massif and/or eastern Sudetes.

Keywords: tourmaline mineral chemistry; Albian sands; heavy-mineral analysis; provenance; Bohemian Massif; Miechów Synclinorium; Poland

1. Introduction

In the history of the Earth, the Cretaceous (145–66 Ma) is considered to have been a very uneventful period in Europe. After the Variscan orogeny (c. 300 Ma) in the Late Palaeozoic, denudation and peneplanation processes of elevated areas took place in extra-Alpine Europe during the Permian, Triassic and Jurassic, and the land was flooded by relatively shallow epicontinental seas [1]. Old structures were rejuvenated only during the Cimmerian tectonic phases [1,2]. Additionally the sea level was controlled by eustatic changes [2]. In the latest Early Cretaceous, in Albian times (earlier than 100.5 Ma), after the neo-Cimmerian tectonic movements phase (c. 145 Ma), a widespread sea transgression took place in epicontinental extra-Alpine Europe. The area of the nowadays Miechów Synclinorium, in the literature commonly called the Miechów Segment of the Szczecin–Miechów Synclinorium [3], is located in southern Poland (Figure 1). That area, during the Middle and Late Albian (110.8–100.5 Ma), was the southern peripheral part of that epicontinental sea and was limited by land and/or islands to the south (Figure 2). In that peripheral, marginal sea zone [4,5], sometimes even in coastal settings [6], siliciclastic sedimentation (mainly quartz sands) dominated [7]. Today, the Albian sands occurring in Poland are intensively mined as raw material for the glass industry in the Tomaszów Mazowiecki

area (the southern part of the Łódź Synclinorium—North of the study area, see Figure 1). Its raw material properties are, due to the very low amount of FeO and TiO₂, reflected in the low content of Fe-Mg-bearing phyllosilicates and very low concentration of heavy minerals containing Fe and Ti, e.g., magnetite, ilmenite, minerals of the TiO₂ group [8–10].

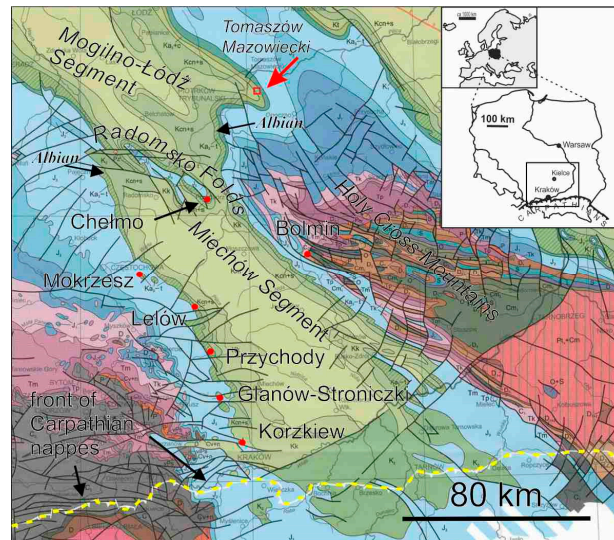


Figure 1. Geological map of the Miechów Segment (southern part of the Szczecin–Miechów Synclinorium) and adjacent areas, southern Poland [11]. Standard stratigraphic colours were used: green—Cretaceous; blue—Jurassic; violet-pink—Triassic; other colours—pre-Mesozoic. Red dots indicate sample localities. Red arrow indicates the mined area for glass industry raw material (informal name Biała Góra deposit) near Tomaszów Mazowiecki. Yellow dotted line shows front of Carpathian nappes.

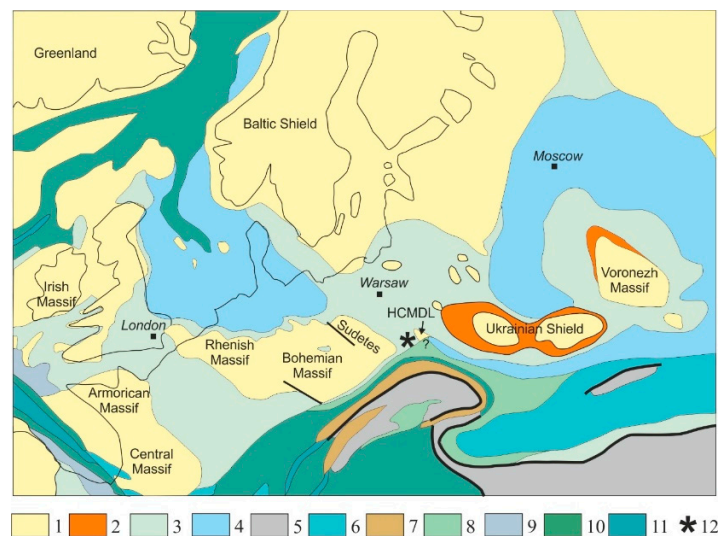


Figure 2. Albian palaeogeography of epicontinental sea and adjacent western Tethys of Europe with simplified distribution of facies (modified from, [1,12]); 1—Land areas; 2—Deltaic, coastal, and shallow marine clastic facies (sands and conglomerates, sands and shales); 3—Shallow-marine facies (sands, marls, carbonate marls, marly carbonates, carbonates); 4—Mainly shallow-carbonate marine facies (marly carbonates, carbonates, chalk, white chalk, carbonate shales); 5—Active fold belts, high relief; 6—Marine carbonates; 7—Deeper marine clastics (sand and shales); 8—Deeper marine carbonates (sands and shales); 9—Carbonates and sands; 10—Deeper marine facies (sands and shales, shales); 11—Deeper marine shale facies (the area of rift); 12—Miechów area; HCMDL—hypothetic Holy Cross Mountains–Dobruja Land; ?—no precise data for the southern edge of the HCMDL.

Sedimentary structures are absent or illegible, or too poorly developed to indicate transport direction/directions of the detrital material to the Albian epicontinental sea [4,6]. Therefore, the chemical analysis of heavy minerals seems to be a promising method in provenance studies of these rocks. Chemical compositions of heavy minerals have been successfully used in the provenance analysis of siliciclastic rocks and in determination of source areas in many places around the world [13–22]. The heavy mineral content in the sandy Albian formation of southern Poland has not yet been subject to detailed examination. A few studies of the Albian sands focused only on the descriptive and quantitative mineralogy [23–26]. The mineralogical data obtained during a preliminary study [27] indicate an abundance of tourmaline, rutile, zircon, monazite, staurolite and muscovite in the Albian clastic sediments. Detrital tourmaline is one of the most abundant heavy mineral in the material examined from the Albian sands of the Miechów Segment and was selected as the first mineral in a series of articles about the provenance of the Albian sands in extra-Carpathian Poland. Tourmaline commonly occurs in sedimentary rocks as a detrital component, often associated with other ultra-stable mineral species, such as zircon and rutile and their concentration, is used in determination of mineralogical maturity of detrital material [28–32].

Tourmaline-supergroup minerals (for simplicity, the short term tourmaline will be used in this paper) is the most common borosilicate mineral found in nature. It occurs mostly as an accessory mineral, seldom being a rock-forming mineral with the exception of rare rocks like metamorphic tourmalinites [33,34]. Tourmaline minerals found in igneous rocks are most often enriched in Fe and/or Mg and are therefore classified as minerals of the schorl-dravite series [35,36]. In igneous rocks, tourmaline is most commonly found in granite pegmatites [37–41] and granites [41–44]. The tourmalines which crystallize in pegmatites are often enriched in Li, F and other elements, such as Mn and Zn [45,46]. Tourmaline in metamorphic rocks crystallize over a wide range from low-grade to ultrahigh-pressure facies conditions, even above 4 GPa [36,47,48]. The tourmaline often occur in metamorphic rocks such as meta-evaporites [49,50], hornfels [51], aluminous schists [52–55], gneisses [56–58], skarns [59] and marbles [60]. Tourmaline can also be found in sedimentary rocks, where it crystallizes in pore spaces during diagenesis [61–63]. The ubiquity of occurrence in various rock forming environments is also reflected in the diverse chemical composition of tourmaline-supergroup minerals [36]. Tourmaline can provide information on the compositional evolution of its host rocks, due to its chemical stability and ability to incorporate a wide range of elements in the structure depending on the formation conditions [64–68].

The very high resistance of tourmaline to both chemical and physical weathering [16], the prevalence of occurrence in igneous and metamorphic rocks and the highly diverse chemical compositions makes this mineral group an excellent tool for determining source areas for detrital material deposited in siliciclastic sedimentary basins [68–70]. The applicability of this tool in provenance analysis is also dependent on mineralogical data for tourmaline found in rocks from hypothetical source areas [34,35,41,44,54,60,67,71].

Although it seems plausible to assume structural highs to be important sediment sources, the exact origin of the Albian deposits was not investigated in detail. The most likely source areas were located in Bohemian Massif, and/or the Ukrainian Shield [1,72,73]. An additional source area, poorly documented by mineralogical research, could be the so-called Holy Cross Mountain–Dobruja Land (HCMDL) [74], otherwise referred to as the Krukienic Island [75], located southeastern of the studied area (Figure 2). The crystalline basement of the southern part of the Fennoscandia Shield, located relatively far away to the north from the Miechów Segment [12], should also be considered as the possible sediment source area (Figure 2).

The aims of this paper are: (1) to comment on the physical properties of tourmaline as an important factor influencing the mode of preservation of tourmalines in detrital settings; (2) to report on the chemical composition of tourmalines from seven outcrops scattered in the Miechów Segment, southern Poland; (3) to compare the composition of the studied tourmalines with that of tourmaline crystals from the assumed source areas; and finally, (4) to point out some of the possible provenances of tourmalines

from the Albian quartz sands to determine both the types of source rocks and the location of source area (s).

2. Regional Geological Setting

The study area is the southern part of the Szczecin–Łódź–Miechów Synclinorium (Figure 1), referred to as the Miechów Segment [3]. The Radomsko Folds [3,76] with Chełmo Mount terminate the Miechów Segment from the north and separate it from the Mogilno–Łódź Segment (Figure 1). Albian deposits crop out only at marginal parts of the Miechów Segment while the central parts are covered by Upper Cretaceous limestones, marls and siliceous chalk [77–80]. The Albian deposits, in the south-western part of the Miechów Segment, form a narrow, longitudinal belt of outcrops (e.g., those studied here are Korzkiew, Glanów–Stroniczki, Przychody, Lelów and Mokrzysz), nearly 100 km long [4,81]. The deposits form white and yellow sands (Figure 3a) and/or loosely lithified sandstones [4,6,81], with a significant amount of glauconite and muscovite. In contrast to the localities from the south-western part of the Miechów Segment, the Albian deposits on the Chełmo Mount [82,83] are exclusively grey, partially ferruginous, lithified quartz sandstones (Figure 3b). These rocks are exposed on the southern slope of the morphological elevation (323 m a.s.l.) in working and abandoned quarries. In the north-eastern part of the Miechów Segment close to the Holy Cross Mountains, as in the south-western part, the Albian deposits also form a narrow, longitudinal belt, but well exposed outcrops are rather rare in that margin [5,72,84]. One of the best known outcrop occurs at Wrzosówka Hill near Bolmin [85]. In the upper part of this section, the Albian deposits are poorly lithified and ferruginous sandstone, while in the lower parts, they are a weakly lithified yellow sandstone and/or loose sand.

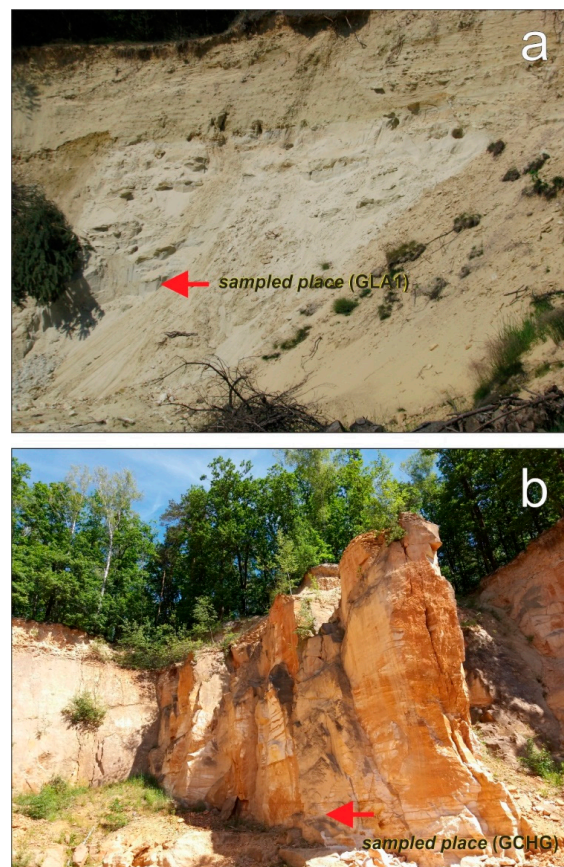


Figure 3. Outcrops of Albian clastic rocks in the Miechów Segment. (a) The wall of loose yellow and white sands in a sandpit at Glanów-Stroniczki, (b) Abandoned quarry of lithified yellow quartz sandstone on top of the Chełmo Mount.

The Albian deposits directly cover Upper Jurassic limestones or calcareous clays [5,82] (Figure 1) and are covered by lithified carbonate Cenomanian deposits [4,5]. The thickness of Albian deposits is variable and ranges from 0 to c. 50 m [4,81] in the south-western part of the Miechów Segment, c. (?) 180 m in Chełmo Mount [82] and approx. 26–76 m in the eastern part [84]. The differences in thickness of the Albian deposits was probably controlled by active synsedimentary block-faulting which played a substantial role in regulating local deposition [4,5]. Among the outcrops studied here, e.g., the thickness of the Albian sands varies and ranges from about 1.5 m in Korzkiew to over 13 m in Glanów–Stroniczki in the western margin of the Miechów Synclinorium.

The Albian sea transgressed directly on the various type of limestones of the Middle/Upper Oxfordian to Lower Kimmeridgian age or calcareous clays of Kimmeridgian age along the margin of the epicontinental Central European Basin [4,81,86,87]. In the Miechów area, the Albian sands accumulated in extremely shallow seas, in nearshore and shore zones [4,6] chiefly as quartz sands over a long distance. The calcareous Jurassic substratum (pure limestones and calcareous clays) cannot have produced sufficient amounts of clastic material for the Albian deposits. Thus, the detrital material was probably transported from an elevated, active terrane and/or island adjacent to the epicontinental Albian sea (Figure 2).

3. Materials and Methods

Sand samples were taken from seven natural outcrops of the Miechów Segment (Figure 1). The five localities (see Figure 1) going progressively from south to north: Korzkiew (KRZ), Glanów–Stroniczki (GLA1) (Figure 3a), Przychody (PRZ), Lelów (LEL) and Mokrzysz (MO) are situated in the south-western part of the Miechów Segment. A single locality is situated at the Chełmo Mount (see Figure 3b) on the northern part of the Miechów Segment (Figure 1), and one outcrop on the southern slope of the Wrzosówka Hill in Bolmin (BOL), in the north-eastern part of the Miechów Segment (Figure 1) was also sampled. In the Chełmo Mount two samples from the lower (GCHD) and upper (GCHG) parts of the section were used (the sections thicker than 20 m) to test difference/similarity between them. From the other six localities only one representative sample from each outcrop was taken for further analytical study.

In order to separate the heavy minerals, a one kilogram sample was used. The two sandstone samples from the Chełmo Mount, before separation, were initially crushed in a Testchem LKS-60 jaw crusher. All eight samples (loose sand and crushed material) were then rinsed with double-distilled water to dispose of the clay fractions and then sieved to obtain 63–125 μm and 125–250 μm size fractions. From these fractions, three magnetic fractions (0.3 A, 1.2 A and a non-magnetic one) were obtained from a single sample after separation on the Franz LB-1 Magnetic Barrier Laboratory Separator. The most magnetic minerals, such as magnetite, Fe-Ti oxides and some garnets tend to concentrate in the 0.3 A fraction while tourmalines and the majority of garnets fall into the 1.2 A group. This procedure not only helps in gaining high quality heavy mineral concentrates but also shortens the time of density separation using a heavy liquid. In this case all obtained fractions were then separated using “LST Fastfloat” heteropolytungstate with a density of 2.9 g/cm^3 . After heavy liquid separation, the tourmaline grains were handpicked and mounted in epoxy resin for electron probe microanalysis (EPMA) investigation. The polished slabs for the EPMA were in the form of one-inch discs, and the surface with exposed tourmaline grains was finally polished using polycrystalline diamond with grains less than 1 μm in diameter.

The crystal surface morphology and initial mineral identification after heavy liquid separations were performed using JEOL JSM-6380 LA and ZEISS SIGMA VP electron microscopes equipped with energy-dispersive X-ray spectrometers (SEM-EDS) in the National Multidisciplinary Laboratory of Functional Nanomaterials NanoFun, Faculty of Geology, University of Warsaw (Warszawa, Poland). The high-resolution scans and elemental mappings were also conducted on the ZEISS SIGMA VP (Carl Zeiss Microscopy, Cambridge, UK) electron microscope. Minerals were identified based on the interpretation of energy-dispersive X-ray spectra of minerals recorded using an electron

microscope coupled with an EDS spectrometer in accordance with the methodology proposed by Severin [88] and on the basis of their mineral chemistry determined by an electron probe microanalysis (EPMA). The chemical composition of tourmaline grains was determined by the wavelength-dispersive spectrometry method (EPMA) using a CAMECA SX-100 electron microprobe at the Joint-Institute Analytical Complex for Minerals and Synthetic Substances, University of Warsaw (Warszawa, Poland). The analyses were done under a 15 keV accelerating voltage, 10 nA beam current and spot size ranging from 2 to 5 μm . The counting times 20 s at peak and 10 s for background were applied. The pure analytical results were finally recalculated using ZAF correction procedures (Z-atomic number correction, A- absorption correction, F- fluorescence correction) [89]. The natural minerals and synthetic compounds supplied by Cameca and Structure Probe, Inc. were used during calibration of the microprobe [90]. The standards, type of diffracting crystal (LIF—crystal made of lithium fluoride, PET—crystal made of pentaerythritol, LPET—large-area diffracting crystal made of pentaerythritol, TAP—crystal made of thallium acid phthalate, PC0—one-dimensional photonic crystal 0 composed of thin W-Si layers), analytical lines used and mean detection limits, expressed in wt%, were as follows: F (synthetic fluorophlogopite, PC0, K_{α} , 0.18), Na (albite, TAP, K_{α} , 0.04), Mg (diopside, TAP, K_{α} , 0.02), Si (diopside, TAP, K_{α} , 0.03), Ca (diopside, PET, K_{α} , 0.02), Al (orthoclase, TAP, K_{α} , 0.03), K (orthoclase, PET, K_{α} , 0.02), Ti (rutile, LPET, K_{α} , 0.02), Mn (rhodonite, LIF, K_{α} , 0.12), Fe (hematite, LIF, K_{α} , 0.13), V (V_2O_5 , LIF, K_{α} , 0.10), Cr (Cr_2O_3 , LPET, K_{α} , 0.03) and Zn (sphalerite, LIF, K_{α} , 0.25). The B_2O_3 , H_2O and Li_2O were calculated by stoichiometry, assuming 3 B apfu (atom per formula unit), $\text{OH} + \text{F} = 4$ apfu and $\text{Li} = 15$ -total ($\text{T} + \text{Z} + \text{Y}$). The amounts of Fe^{3+} , Fe^{2+} , and H_2O , in the form of OH groups, were calculated by stoichiometry based on the electroneutrality of the tourmaline formulae. The complete set of analytical data is provided in the Supplementary Materials (see Table S1: Chemical composition of tourmaline from the Albian sands in the Miechów Synclinorium).

4. Results

The loose material from Korzkiew, Glanów–Stroniczki, Przychody, Lelów, Mokrzysz and Bolmin comprised of well sorted, medium- and fine-grained sands (0.1–0.5 mm grain diameter, with dominant grains in the range 0.2–0.3 mm). Small amounts of a gravel component are present. Most grains in the sandy fraction are subangular, some are subrounded and only a few are rounded. The sands consist of quartz (90%), glauconite (1–6%), feldspar (1–3%), muscovite (0.2–2%) and other detrital grains including the heavy minerals are less than 1%.

The framework of sandstone from the Chełmo Mount (Figure 4) is also comprised of well sorted medium and fine grains (0.1–0.5 mm with dominant grains of 0.2–0.3 mm). A gravel fraction is also present, and commonly forms irregular lenses, up to 10 cm thick. Most grains are subangular, only rare grains are subrounded (Figure 4). The grains are quartz (c. 98%), K-feldspar (less than 1%), glauconite (less than 0.5%), muscovite (seldom, only singular flakes found) and other detrital grains, including the heavy minerals (less than 1%). This points to the petrographic similarity between sandstones from the Chełmo Mount and loose sands from the other examined outcrops. The sandstone is cemented chiefly by chalcedony and additionally by clay minerals (kaolinite) and can be classified as a quartz arenite. It is worth noting that sandstone from the Chełmo Mount is highly porous.

As shown above, the mineralogical composition of loose sands and sandstones from the different outcrops of the Miechów Segment is very similar and the differences are negligible. In the Chełmo Mount the quartz content reaches up to 98% of all detrital grains while in the other outcrops it is about, or slightly less than, 90%. The quartz grains are monocrystalline and less frequently polycrystalline. Glauconite grains can be found in every studied sample. Its concentration varies from less than 0.5% in sandstones from the Chełmo Mount, up to 6% of all grains in Glanów–Stroniczki or Bolmin. In some samples from outcrops exposed for a long time, glauconite tended to change its colour from green to greenish-yellow due to oxidation and weathering. Among the feldspars the K-feldspar dominate over rare Na-plagioclase. Large flakes of muscovite, up to 5 mm in diameter, can be found in the

south-western part of the study area in samples from Glanów-Stroniczki and Lelów. Finer muscovite flakes are present in all other localities.

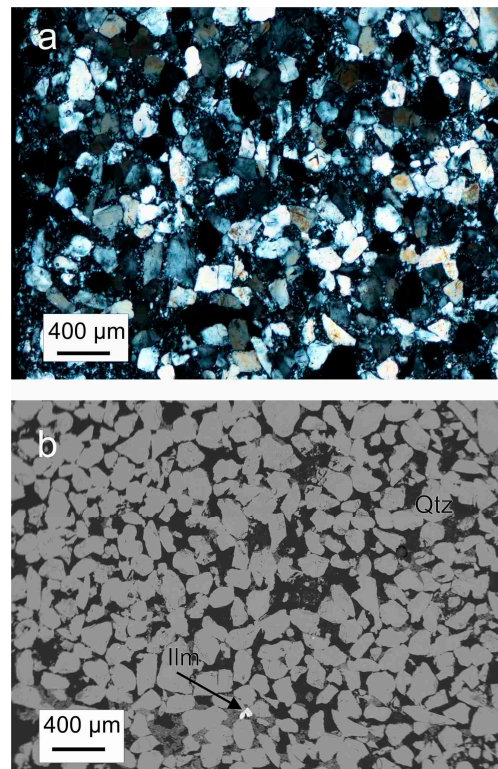


Figure 4. Petrography of the quartz sandstone from the Chełmo Mount. (a) Fine- to medium-grained, well sorted quartz sandstone, cemented by siliceous cement, polarized light microscopy image, crossed nicols; (b) SEM-BSE (Scanning Electron Microscope-BackScattered Electron) image of the same sample area; Ilm—ilmenite; Qtz—quartz.

The heavy mineral assemblages found in the Albian sands from the Miechów Segment are dominated by Fe-Ti oxides (ilmenite, leucoxenized to varying degrees), zircon, tourmaline, rutile and staurolite. The subordinate minerals found in the samples are garnet, Al_2O_3 neosilicate polymorphs (mainly kyanite and sillimanite) and monazite. The additional minerals that can be found in the samples in the smallest amounts were gahnite, chromium spinel, xenotime, titanite, cassiterite and biotite. A few broken biotite flakes, 50–100 μm in diameter, were found only in the south-western part of the examined area. The assemblages of heavy minerals from all studied samples are quite similar to each other. It is worth noting here that easily weathered minerals, such as amphibole, pyroxene and Ca-plagioclase, are absent and were not encountered in any of the localities. It is also interesting that apatite, which commonly occurs in detrital settings, is also absent.

Tourmaline is one of the major heavy minerals (up to 20% of the entire heavy mineral assemblage) occurring in the Albian sands and sandstones of the Miechów Segment. The most frequent tourmaline types are brown and black in colour. Colourless or light yellow tourmaline grains are subordinate. The crystal size is variable and, on average, ranges from approx. 30 to 250 μm . Grains larger than 500 μm are rare and often rounded. Under the scanning electron microscope (SEM), most of the tourmaline grains are euhedral, only partially cracked, angular, subangular and subrounded in shape (Figure 5a–c). A slight degree of abrasion can be distinguished on the grain surfaces. The edges and joints of the walls are often abraded to the higher degree than the wall surfaces (Figure 5). The rounded and well-rounded tourmalines are less common (Figure 5d) and constitute only from 4 to 15% of all tourmaline grains.

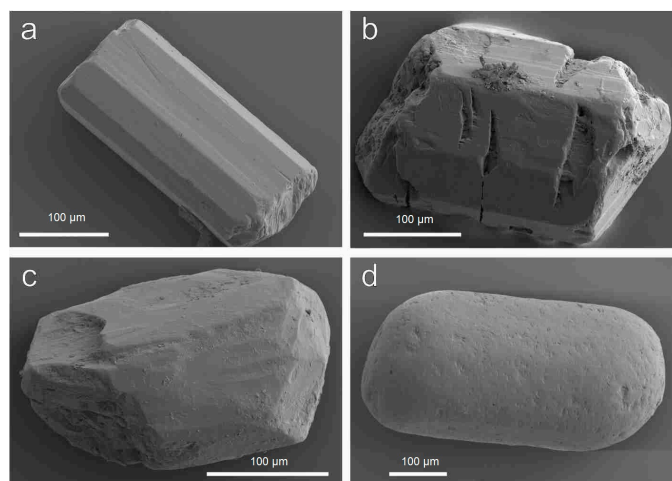


Figure 5. SEM–SE (Scanning Electron Microscope–Secondary Electron) images of tourmaline types in terms of their roundness and deterioration degree; (a) Angular grain, Glanów–Stroniczki, (b) Subangular grain with etchings, Lelów, (c) Subrounded grain, Mokresz, (d) Rounded grain, Korzkiew; scale bars are 100 µm.

Tourmaline is a complex borosilicate with a general formula $XY_3Z_6T_6O_{18}(BO_3)_3V_3W$ [68]. X-site is predominantly occupied by Na^+ , Ca^{2+} or with a significant vacancy (\square), minor amounts of K^+ can also be present. Tourmaline is classified into three primary groups: alkali-, calcic- and X-site vacant, based on the X site occupancy [20,36]. The Y-site forms an octahedral polyhedron that may be occupied by a wide range of multivalent cations: Li^+ , Mg^{2+} , Fe^{2+} , Mn^{2+} , Al^{3+} , Cr^{3+} , V^{3+} , Fe^{3+} and Ti^{4+} . The small Z-site is occupied by trivalent cations such as Al^{3+} , Fe^{3+} , Cr^{3+} and V^{3+} but can also contain significant amounts of Mg^{2+} [50]. The tetrahedral T-site is mainly filled with Si and usually filled by excess of Al^{3+} and B^{3+} which fully occupy the triangularly coordinated B-site. The V-site chiefly contains an OH^- group but can also have significant amounts of O^{2-} while the W-site exclusively contain F^- with excess O^{2-} and OH^- .

Over 512 tourmaline grains from the Miechów Segment were analysed using EPMA (Table 1 and Table S1). The majority of grains belong to the alkali tourmaline group in which the X-site is dominated by Na and to lesser extent K [36]. Sodium is the most abundant cation in the X site, ranging from 0.4 to 0.9 apfu (atom per formula unit). Potassium concentrations are very low and in most cases its concentrations are below detection limit. In only a few grains K reaches 0.1 apfu. The X-site vacancy values ranges from 0.02 to 0.6 apfu but usually are lower than 0.3 apfu. Therefore, only 5% of all tourmaline crystals can be classified as vacancy group tourmalines in which foitite significantly outweighs the Mg-foitite. Calcium rarely exceeds 0.1 apfu, so only two grains can be considered as uvite, a Ca-group tourmaline (Figure 6). The two dominant divalent cations in the Y-site are Mg and Fe; thus, most of the analysed tourmalines can be classified as of the schorl–dravite series (Figure 6). The high $X_{Mg} = Mg/(Mg + Fe)$ ratio (avg. 0.6) within the alkali group indicates that Mg is the main cation in the Y-site. Therefore nearly 70% of all tourmaline grains found in the sands and sandstones studied here are classified as dravite. Other analysed cations that occupy the Y-site, such as Ti, Mn, V, Zn and Cr, rarely exceed 0.1 apfu (Table 1). Titanium concentrations reach a maximum of 0.27 apfu. An exception is a single, green grain of dravite from Bolmin (Table 1), in which significantly elevated V and Cr contents (respectively 1.25 and 0.48 apfu) were noted. The Z-site, in the vast majority of tourmaline grains, is entirely filled by Al. In rare cases of a small Al deficiency (less than 0.1 apfu), this position is supplemented by Mg. The fluorine content is usually below detection limit; however, in some grains, this can reach up to 0.7 apfu (Table 1). The high amounts of F are mostly found in dravite, however, there are also cases of schorls rich in fluorine. There is no significant correlation of elevated F content with the location of the sample.

Table 1. Cont.

Locality	Lelów (LEL)				Przychody (PRZ)				Chelmo Mount Lower Part (GCHD)				Chelmo Mount Upper Part (GCHG)			
Sample	LEx14	LEx20	LEx47	LEx64	PRx1	PRx10	PRx24	PRx29	GCDx11	GCDx29	GCDx36	GCDx55	GCGx5	GCGx25	GCGx26	GCGx55
SiO ₂	37.23	36.84	35.58	34.81	35.16	36.0	36.48	37.27	34.32	35.54	36.32	36.15	36.02	38.1	36.68	37.89
TiO ₂	0.66	0.66	0.62	0.79	0.39	0.28	0.65	0.35	0.7	0.87	0.77	0.76	0.51	0.13	1.21	0.03
B ₂ O ₃ *	10.83	10.65	10.46	10.5	10.49	10.59	10.83	10.74	10.08	10.71	10.7	10.68	10.62	10.93	10.62	10.96
Al ₂ O ₃	33.14	32.33	33.19	26.07	34.36	34.47	34.82	32.1	30.01	34.85	34.11	34.07	34.52	32.43	30.76	36.07
V ₂ O ₃	0	0	0	9.4	0	0.03	0	0.06	0	0.14	0.03	0.08	0	0	0	0
Cr ₂ O ₃	0.05	0.08	0	3.67	0	0	0.06	0.06	0	0.04	0.09	0.08	0	0	0.06	0
FeO	5.61	7.43	11.77	0.27	9.74	9.54	3.62	4.56	16.07	5.53	6.46	6.65	10	1.61	6.28	5.78
MgO	7.58	6.26	3.02	8.11	3.85	3.85	7.39	8.6	1.91	6.2	5.9	5.88	3.63	10.63	7.8	5.63
MnO	0	0	0.13	0	0	0.15	0	0	0	0.11	0.13	0	0	0	0	0
CaO	0.21	0.29	0.23	1.3	0.28	0.24	1.18	0.11	0.76	0.92	0.35	0.34	0.15	0.23	0.66	0.11
Na ₂ O	2.34	2.36	2.03	1.75	1.97	1.82	1.59	2.73	2.16	1.68	1.89	1.95	1.87	2.94	2.5	1.493
K ₂ O	0.02	0	0.03	0.1	0.05	0.04	0.06	0.04	0.09	0.07	0.04	0.04	0.04	0.02	0.04	0.02
F	0	0	0.33	0.1	0	0.12	0.12	0.83	0.45	0	0.32	0.35	0	1.41	0	0
H ₂ O *	3.72	3.68	3.45	3.57	3.62	3.59	3.68	3.31	3.26	3.69	3.54	3.52	3.66	3.11	3.66	3.78
O = F	0	0	0.14	0.04	0	0.05	0.05	0.35	0.19	0	0.13	0.15	0	0.59	0	0
Total	101.39	100.58	100.84	100.44	99.91	100.72	100.48	100.76	99.81	100.35	100.65	100.55	101.02	101.54	100.27	101.76
									T-site							
Si ⁴⁺	5.977	6.010	5.911	5.761	5.827	5.910	5.855	6.032	5.920	5.770	5.901	5.884	5.897	6.058	6.004	6.007
Al ³⁺	0.023	0	0.089	0.239	0.173	0.090	0.145	0	0.080	0.230	0.099	0.116	0.103	0	0	0
									Y-, Z-site							
Al ³⁺	6.248	6.217	6.411	4.845	6.538	6.578	6.441	6.122	6.021	6.437	6.432	6.420	6.558	6.077	5.934	6.740
Ti ⁴⁺	0.08	0.084	0.078	0.099	0.049	0.032	0.079	0.043	0.091	0.106	0.094	0.093	0.062	0.015	0.148	0.003
Cr ³⁺	0.006	0.010	0	0.480	0	0	0.008	0.008	0	0.004	0.011	0.01	0	0	0.007	0
V ³⁺	0	0	0	1.248	0	0.004	0	0.008	0	0.018	0.004	0.01	0	0	0	0
Fe ²⁺	0.753	1.014	1.635	0.037	1.350	1.310	0.486	0.617	2.318	0.750	0.878	0.905	1.369	0.214	0.860	0.767
Mn ²⁺	0	0	0.018	0	0	0.021	0	0	0	0.015	0.018	0	0	0	0	0
Mg ²⁺	1.815	1.523	0.749	2.001	0.951	0.941	1.767	2.075	0.491	1.50	1.429	1.426	0.887	2.519	1.903	1.330
Subtotal	8.902	8.848	8.891	8.710	8.888	8.886	8.781	8.873	8.921	8.83	8.866	8.864	8.876	8.825	8.852	8.840
									X-site							
Ca ²⁺	0.036	0.051	0.041	0.231	0.049	0.041	0.202	0.020	0.140	0.161	0.061	0.060	0.025	0.039	0.115	0.019
Na ⁺	0.728	0.748	0.655	0.560	0.634	0.579	0.496	0.856	0.721	0.530	0.596	0.614	0.592	0.905	0.794	0.459
K ⁺	0.005	0.002	0.006	0.020	0.010	0.009	0.012	0.008	0.019	0.015	0.008	0.008	0.009	0.005	0.008	0.004
Vacancy	0.231	0.199	0.298	0.188	0.308	0.371	0.290	0.116	0.121	0.294	0.335	0.318	0.374	0.051	0.083	0.519
OH ⁻	4	4	3.829	3.946	4	3.937	3.938	3.576	3.753	4	3.837	3.822	4	3.294	4	4
F ⁻	0	0	0.171	0.054	0	0.063	0.062	0.424	0.247	0	0.163	0.178	0	0.706	0	0

* B₂O₃, and H₂O were calculated by stoichiometry, assuming 3 B apfu, OH + F = 4 apfu, based on electroneutrality of the tourmaline formulae.

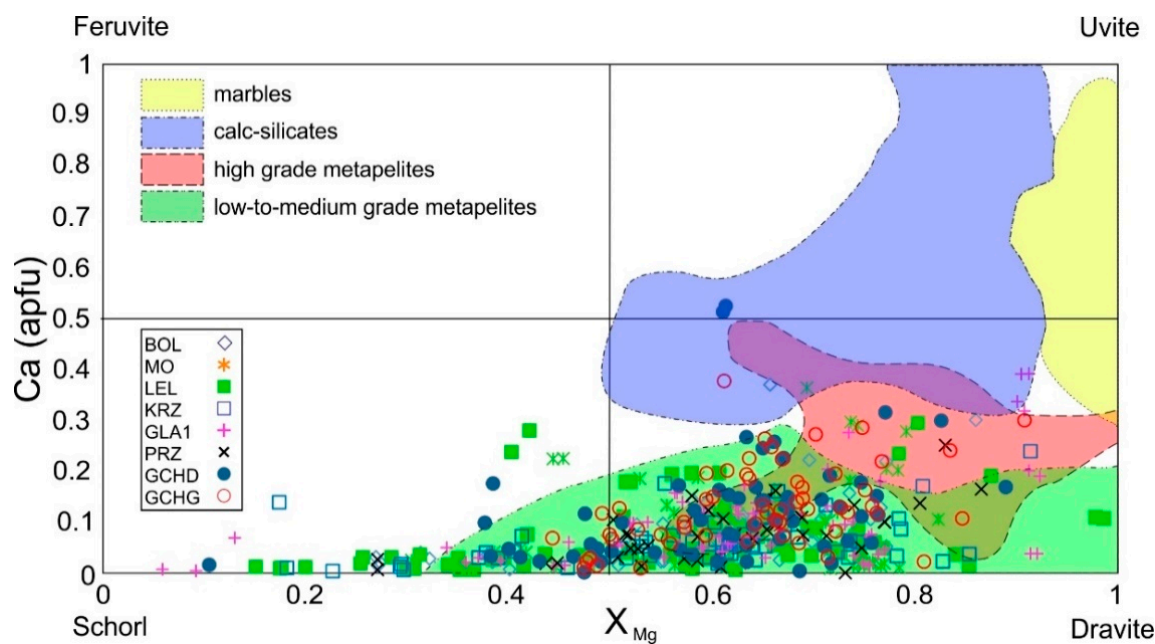


Figure 6. X_{Mg} vs Ca discrimination diagram of Henry and Dutrow [91] showing mineral chemistry of the examined tourmaline grains from the Albian sands of the Miechów area.

Most of the detrital tourmaline grains are compositionally homogenous, but some distinctly zoned tourmalines (Figure 7) were present in all studied samples. The changes in composition are quite distinct (Table 2) and are visible in BSE images; however, in some cases faint zones were visible only after elemental mapping in SEM-EDS (Figure 7). In these cases, Fe, Mg and sometimes Ca maps were the most helpful in distinguishing subsequent zones. The inner cores of zoned tourmalines do not show a clear pattern in chemical composition. Twenty-two analysed grains have Mg-rich, dravite cores (Figure 7e–h), while in the remaining 18 grains, the inner core was enriched in Fe (schorl-like cores, Figure 7a–d). Four different zones (I–IV) are visible in the case of a grain from the Glanów-Stroniczki (Figure 7a–d). The inner core (zone I) has a schorl-like composition with the highest concentrations of iron. The subsequent zone II also has schorl-like composition but with larger Mg content. Zone II has a very distinctive asymmetrical pattern. These two inner zones (I and II) are quite similar to each other. In contrast, zone III has a dravite-like composition, with Mg dominating over Fe and high concentrations of Ca (Table 2). Large quartz intergrowths are also visible in this zone. Zone IV, being the outer rim of the crystal, is similar in composition to zone III. The only major difference is in the lower amounts of Ca (Figure 7c) and the lack of quartz intergrowths.

The percentage distributions of tourmaline species are quite similar between samples in the south-western part of the Miechów Segment. The dravite is, on average, about 70–80% and schorl about 15% of all tourmaline grains. A larger percentage of schorl, on average around 20%, is noted in samples from Bolmin and the Chełmo Mount. Tourmaline from the vacancy group, i.e., foitite and Mg-foitite, account for up to 5–7%, regardless of locality. It is worth noting that there was no difference in chemical composition between the rounded and the euhedral tourmalines from the same sample.

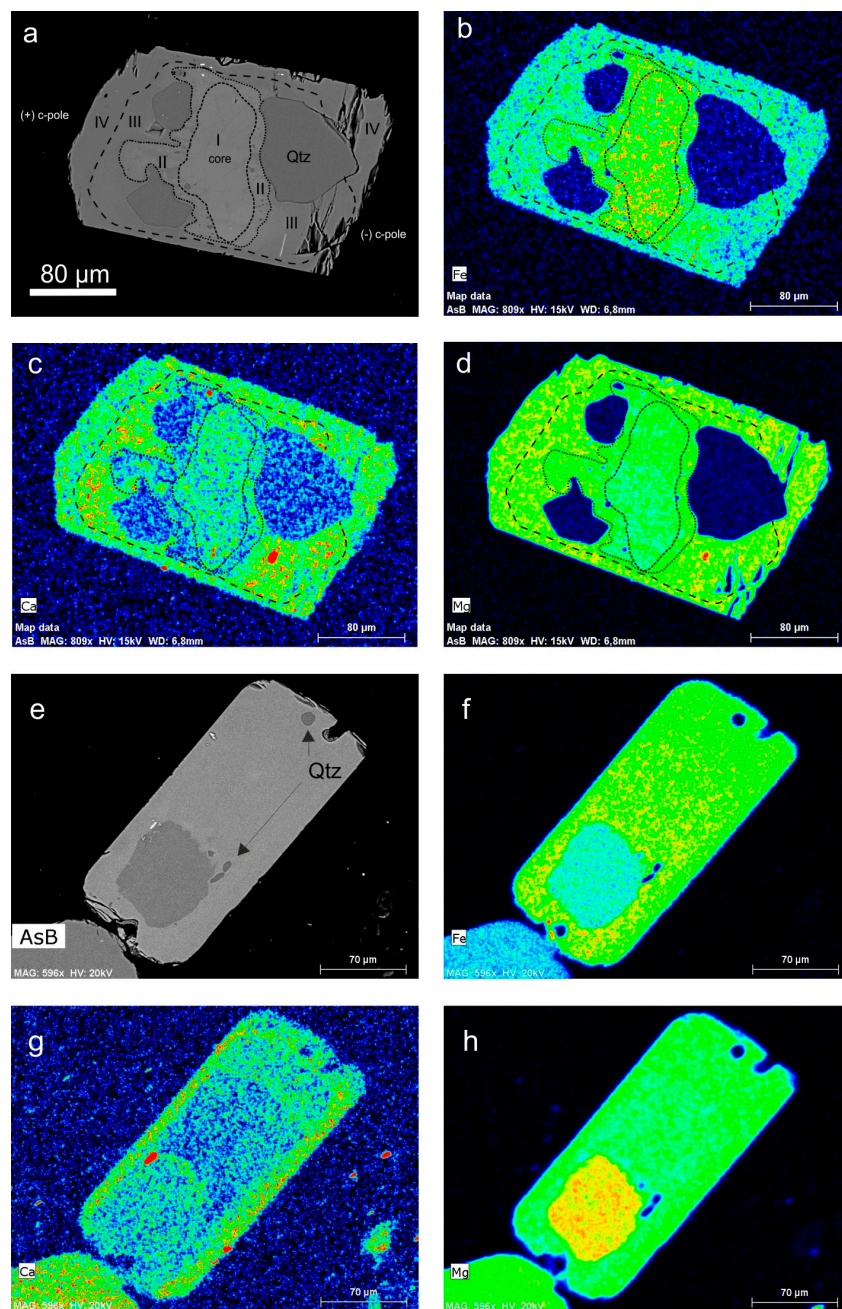


Figure 7. SEM-BSE images and elemental maps of zoned tourmaline grains from the Miechów Synclinorium showing their multi-stage growth. (a–d) detrital tourmaline grain from Glanów–Stroniczki: (a) SEM-BSE image, distinct chemical zonation (I–IV) is underlined with dotted lines; (b–d) distribution maps of Fe (b), Ca (c) and Mg (d). (e–h) detrital tourmaline from Lelów: (e) SEM-BSE image of tourmaline grain with clearly visible growth zones. The core of the grain is strongly enriched in Mg, (f–h) distribution maps of Fe (f), Ca (g) and Mg (h). All Elemental maps with false colour scale; dark blue—lowest concentrations, red—highest concentrations of analysed element; Qtz—quartz.

Table 2. Mineral chemistry of distinguished zones (I–IV) in multistage tourmaline grain from Glanów–Stroniczki.

Locality	Zone I				Zone II				Zone III				Zone IV			
Point	1	2	3	4	5	6	7	8	9	10	11	12	13	14		
SiO ₂	36.69	36.40	36.44	36.26	36.64	37.91	37.05	36.97	36.94	36.39	37.19	37.19	37.20	36.63		
TiO ₂	1.12	0.93	1.35	0.58	1.032	0.31	0.61	0.64	0.66	0.74	0.76	0.72	0.65	0.69		
B ₂ O ₃ *	10.71	10.68	10.67	10.76	10.67	10.74	10.68	10.83	10.75	10.73	10.79	10.85	10.93	10.7		
Al ₂ O ₃	32.35	33.01	31.67	32.73	32.28	31.98	32..13	32.80	32..51	32..42	31.98	32..51	32..40	32..19		
Cr ₂ O ₃	0.09	0.10	0.14	0	0.08	0	0	0.05	0	0.08	0	0	0.04	0		
FeO	6.55	7.39	6.77	5.05	6.73	7.51	6.93	4.81	4.29	4.74	5.23	4.69	4.65	4.46		
MgO	6.98	6.23	7.18	8.80	6.76	6.61	6.98	8.46	8.36	8.50	8.38	8.64	8.75	8.57		
MnO	0	0	0.16	0	0	0.07	0.06	0	0.04	0	0	0.01	0	0		
CaO	0.57	0.45	0.78	1.19	0.55	0.17	0.32	1.21	1.16	1.37	1.37	0.89	0.75	0.99		
Na ₂ O	2.15	2.01	2.13	1.86	2.18	2.28	2.24	1.81	1.95	1.86	1.75	2.26	2.33	2.11		
K ₂ O	0.05	0.04	0	0	0.03	0	0.05	0	0.05	0	0	0	0.04	0.04		
F	0	0	0	0	0	0	0	0	0	0	0.19	0	0.17	0		
H ₂ O *	3.7	3.69	3.68	3.71	3.68	3.71	3.69	3.74	3.71	3.7	3.63	3.74	3.66	3.69		
O = F	0	0	0	0	0	0	0	0	0	0	0.08	0	0.07	0		
Total	100.96	100.93	100.97	100.94	100.63	101.29	100.74	101.32	100.42	100.53	101.35	101.5	101.64	100.07		
	T-site															
Si ⁴⁺	5.954	5.922	5.933	5.857	5.966	6.135	6.027	5.934	5.970	5.896	5.991	5.958	5.968	5.948		
Al ³⁺	0.046	0.078	0.067	0.143	0.034	0	0	0.066	0.030	0.104	0.009	0.042	0.032	0.052		
	Y-, Z-site															
Al ³⁺	6.142	6.251	6.010	6.087	6.162	6.099	6.161	6.141	6.163	6.086	6.063	6.094	6.094	6.110		
Ti ⁴⁺	0.137	0.114	0.166	0.071	0.126	0.037	0.074	0.078	0.081	0.091	0.092	0.0887	0.079	0.084		
Cr ³⁺	0.011	0.013	0.018	0	0.011	0	0	0.006	0	0.010	0	0	0.006	0		
Fe ²⁺	0.889	1.005	0.922	0.683	0.917	1.016	0.943	0.645	0.580	0.643	0.704	0.628	0.624	0.606		
Mn ²⁺	0	0	0.004	0.001	0.004	0.002	0	0.001	0.002	0	0	0.010	0	0.004		
Mg ²⁺	1.688	1.512	1.743	2.119	1.641	1.593	1.692	2.024	2.013	2.054	2.012	2.064	2.091	2.075		
Subtotal	8.867	8.895	8.863	8.961	8.861	8.747	8.870	8.895	8.839	8.884	8.871	8.8847	8.894	8.879		
	X-site															
Ca ²⁺	0.100	0.078	0.135	0.205	0.095	0.029	0.056	0.207	0.201	0.238	0.236	0.153	0.129	0.172		
Na ⁺	0.677	0.632	0.672	0.583	0.688	0.715	0.706	0.563	0.61	0.585	0.547	0.701	0.723	0.664		
K ⁺	0.011	0.008	0	0	0.007	0	0.010	0	0.010	0	0	0	0.008	0.008		
vacancy	0.212	0.281	0.193	0.212	0.210	0.256	0.228	0.230	0.180	0.177	0.217	0.146	0.141	0.156		
OH ⁻	4	4	4	4	4	4	4	4	4	4	3.902	4	3.914	4		
F ⁻	0	0	0	0	0	0	0	0	0	0	0.098	0	0.086	0		

* B₂O₃, and H₂O were calculated by stoichiometry, assuming 3 B apfu, OH + F = 4 apfu, based on electroneutrality of the tourmaline formulae.

5. Discussion

The Albian sands and sandstones in the Miechów Segment consist of sedimentologically, mineralogically and petrographically mature detrital material. The heavy minerals are scarce in the Albian sands and sandstones and their concentrations are much less than 1%. Tourmaline is a very resistant mineral during weathering and diagenetic processes [16] and therefore counts as a major constituent of heavy mineral assemblages in our samples, together with rutile, zircon, garnet, spinel group minerals, staurolite, kyanite and muscovite.

The Albian sea transgressed onto the Upper Jurassic pure limestone (platy and biohermal) or calcareous clay basement [72,92,93] and only locally onto Lower Cretaceous clays and sands [94,95]. The dominant well sorted detrital quartz in psammitic fraction with an admixture of gravel quartz grains suggest that the source material for Albian sands was different than the Jurassic or Lower Cretaceous basement.

As a common mineral in detrital material, tourmaline is frequently used as a tool in provenance studies [34,35,44,55,60,64–68]. Henry and Guidotti, [69] created a ternary Fe–Al–Mg diagram with discrimination fields reflecting the composition of tourmaline crystallized in different rock types. Most of our results fit well in fields 4 and 5 of the diagram (Figure 8), which correspond to metapelites and metapsammities coexisting and non-coexisting with an Al-saturated phases. However, a certain part of the compositions is located in the field of Li-poor granitoids as well as pegmatites and aplites associated with them. This tourmaline type was documented in samples from Lelów, Korzkiew and

Glanów–Stroniczki (Figure 8). On the other hand, only a small part of the analysed grains tend to fit into low-Ca metaultramafites and Cr-, V-rich metasediments. The distribution of most of the points reflecting the composition of the examined tourmalines on the classification diagram (Figure 8) and the high $Mg/(Mg + Fe)$ ratio (X_{Mg}) of the analysed tourmaline with low values of calcium and vacancy at X-site (Figures 6 and 9), point to a metamorphic origin [91,96].

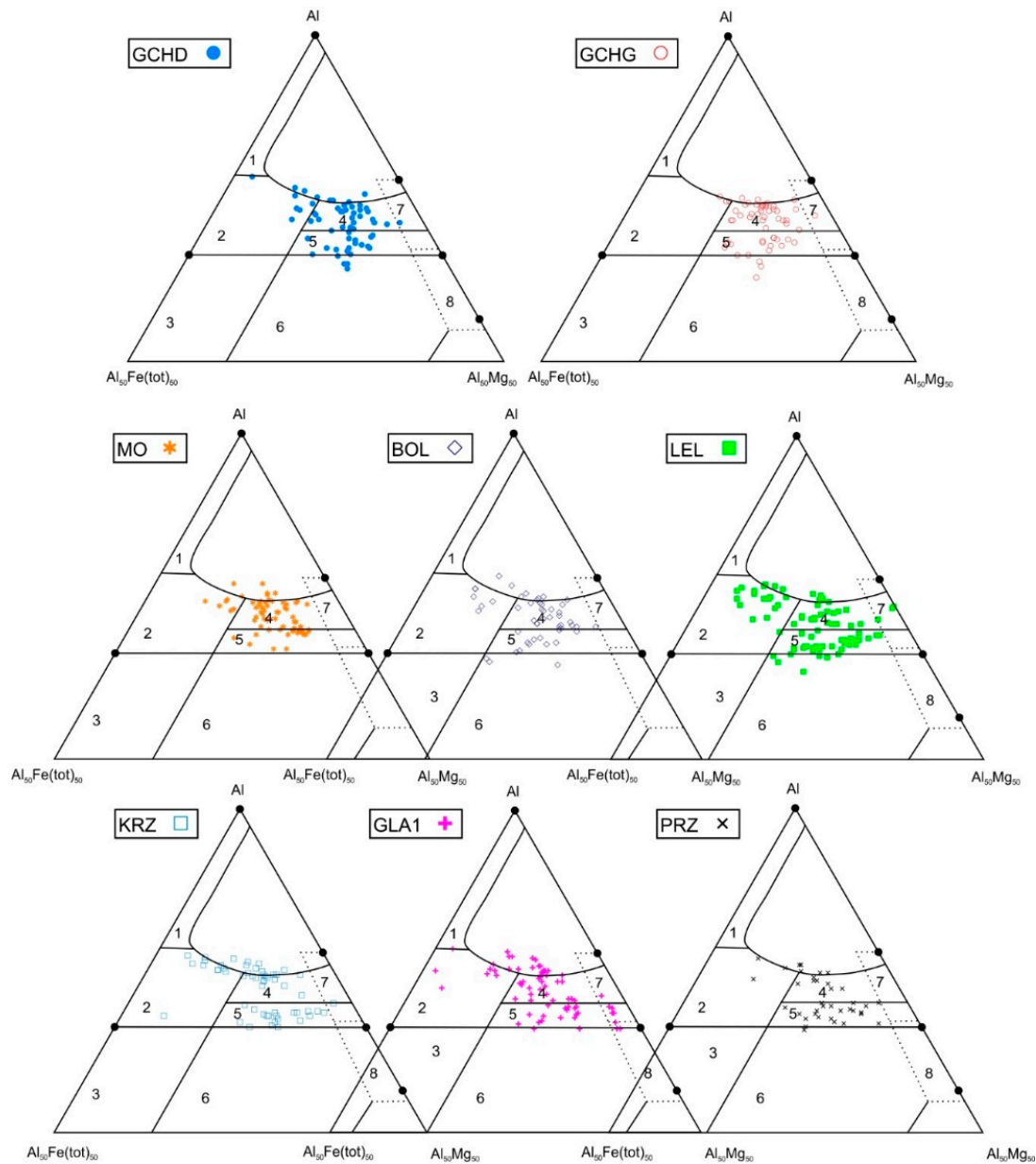


Figure 8. Fe–Al–Mg ternary discrimination diagrams of Henry and Guidotti [69] showing compositions of tourmaline from the Miechów Segment, southern Poland. The distinguished discrimination fields are: (1) Li-rich granitoid pegmatites and aplites; (2) Li-poor granitoids and their associated pegmatites and aplites; (3) Fe^{3+} -rich quartz-tourmaline rocks (hydrothermally altered granites); (4) Metapelites and metapsammites coexisting with an Al-saturating phase; (5) Metapelites and metapsammites not coexisting with an Al-saturating phase; (6) Fe^{3+} -rich quartz-tourmaline rocks, calc-silicate rocks, and metapelites; (7) Low-Ca metaultramafics and Cr, V-rich metasediments; (8) Metacarbonates and meta-pyroxenites.

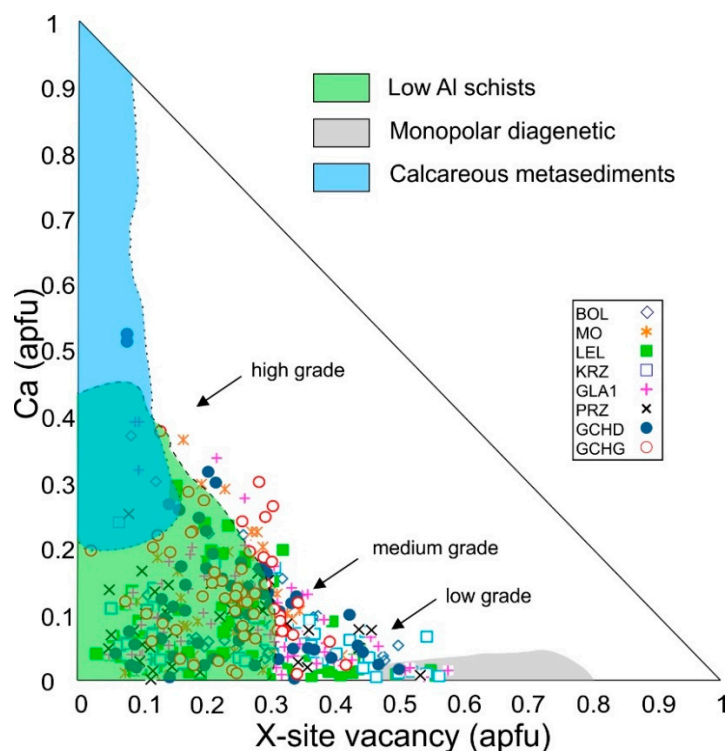


Figure 9. X-site vacancy vs. Ca diagram of Henry and Dutrow [91] used for discrimination of tourmaline grown in low Al schist, calcareous metasediment, and during diagenesis in sedimentary rocks (monopolar diagenetic tourmaline). Points on the diagram reflect mineral chemistry of the examined tourmaline grains.

The tourmalines from metapelites are characterized by a high value of X_{Mg} , oscillating between 0.4–1.0 (Figure 6), and a vacancy at the X-site below 0.6 apfu (Figure 9). The X_{Mg} ratio of all the examined tourmaline grains ranges from 0.57 to 0.64, which fits well to the composition of tourmaline that crystallized in rocks experiencing low- to medium-grade metamorphism. The tourmalines from Albian sands have a vacancy at the X-site on avg. 0.25 apfu (Figure 9) and co-occur with other metamorphic Al-bearing minerals like staurolite, sillimanite and kyanite. This can also be interpreted as indirect evidence of a metamorphic origin for the tourmaline grains [91].

Tourmaline is stable under very diverse pressure-temperature (P-T) conditions from diagenetic [61,62,97], hydrothermal epigenetic [98–101] and through wide range of metamorphic grades [91,102], up to ultra-high pressure (UHP) and high-temperatures [66,103,104]. The thermal stability of the dravite structure was experimentally established up to 3–5 GPa and a temperature close to 950 °C [103]. High pressure (HP) and UHP tourmaline shows an increase of Al in the T-site, an increase of Na, Ca and K contents, a decrease of vacancies at the X-site, and increase of Ti at the Y-site as a reflection of high temperatures of tourmaline crystallization [66,104,105]. Therefore, it is less probable that the analysed tourmalines from the Albian sands could have originated from high-grade metamorphic rocks (Figure 9). Such tourmalines are characterized by an increased content of F (above 0.4 apfu) and high Ca and K contents (up to 0.5 apfu). The features of tourmaline from the Albian sand/sandstone, studied here, such as relatively low Ca contents with the highest values up to 0.38 apfu (avg. 0.13 apfu) and very low concentrations of F, usually below the detection limit (Table 1), point to low- and medium-grade metamorphism, most likely amphibolite facies conditions. Additionally, tourmaline rarely grows in rocks metamorphosed under high-grade granulite facies conditions [68,105], possibly due to a deficiency of B in the fluids generated during this metamorphism. Thus, the most probable source rocks for the Albian sands were ortho- and paragneisses and/or Al-rich quartz-muscovite schists, recrystallized at P-T conditions under low- to medium-grade (amphibolite

facies) metamorphism. This interpretation is supported by the abundant presence of staurolite and muscovite in the heavy mineral association.

Zoned tourmalines occur commonly in metapelites and gneisses [106] and also in various types of pegmatites [107,108]. The tourmaline grains with distinct asymmetric chemical zoning indicate a diagenetic and/or low-grade metamorphic origin [91]. The asymmetrical zonation (e.g., zone II, which has very distinctive asymmetrical pattern) observed in a few grains (Figure 7) from the south-western part of the Miechów Segment, additionally indicates the provenance of tourmaline from low- to medium-grade metamorphic rocks which is in agreement with data shown on the discrimination diagram of Henry and Guidotti [69] (Figure 8) and with Ca- X_{Mg} diagram [91] (Figure 6). The simple zonation discovered in the analysed samples differs from the complex zonation recently described by Konzett et al. [109] and Aubrecht et al. [110] in tourmaline from eclogites from the Eastern Alps (Austria) and from the Cretaceous exotic flysch of the Western Carpathians, respectively. According to these authors, the complex zonation in tourmaline may be an indicator of its growth under HP or UHP metamorphism conditions. However, such a zonation type can also occur in tourmaline from hydrothermal veins, granitoids and metaevaporites [110].

It is worth mentioning other heavy minerals occurring (staurolite, kyanite) or absent (apatite, amphibole, pyroxene, Ca-plagioclase) in the Albian sands/sandstones. Staurolite is a minor but quite ubiquitous accessory mineral found in rocks that underwent medium-grade regional metamorphism, for example gneisses or schists [111,112]. The presence of kyanite may point to high-grade metamorphism, but it could also have crystallized in a thermal aureole near igneous intrusions [113,114]. Apatite was not found in any of the studied samples. It is considered to be a common accessory mineral in a variety of igneous and metamorphic rocks [115]. It is also a stable mineral in marine sediments [16]. Thus, this mineral is commonly found as a detrital component in sedimentary rocks. The absence of apatite can be explained in two ways: either it was not present in the source rock, which is very unlikely, or it was removed from the sediment after deposition. Apatite is a subject of intense chemical weathering in coastal and marginal marine environments as a result of acid groundwater action [116–118]. For this reason, apatite is a good environmental indicator. The absence of this mineral in the studied detrital rocks gives credence to the hypothesis of relatively shallow, coastal or even beach conditions during the deposition of clastic material of the Albian sands which is supported by sedimentology and palaeoichnology studies [4,6]. The unstable minerals, such as amphibole, pyroxene and Ca-plagioclase, experienced dissolution processes during diagenesis, while ilmenite was transformed into polycrystalline leucoxene aggregates mainly composed of anatase. Muscovite was identified in varying amounts in all analysed samples. A significant accumulation of large grains of muscovite (up to 5 mm in diameter) may indicate a pegmatite or metamorphic origin of the source rock. The muscovite flakes are larger and more frequent in the south-western part of the Miechów Segment, in comparison to the rare presence of muscovite in the north-eastern and northern parts of the studied area. This suggests that the south-western part of the Miechów Segment was situated closer to the assumed source area than their north-eastern and northern parts. However, the presence of the large flakes of muscovite can be a result of the hydraulic sorting [119] during transport of detrital material. The size of the muscovite flakes can be controlled by sedimentation dynamics rather than proximity to the source.

On the basis of the composition of the tourmaline grains it can be stated that they come mainly from Al-bearing schists and gneisses metamorphosed under low- to medium-grade conditions; to a lesser extent, their compositions indicate a source in granites and pegmatites. The question then arises: where was the source area for sands of the Miechów area during the Late Albian? If we look at the Albian palaeogeography of central Europe (Figure 2), the nearest sediment source area(s) with the rock types mentioned above (i.e., mica schists, gneisses and granites) can be found in the Bohemian Massif [41,120,121]. However, in most cases tourmalines present in rocks exposed in the Sudetes (N part of Bohemian Massif) are mainly Fe-dominant schorl [35,122]. The other potential source area may be the southern extension of the hypothetical Holy Cross Mountain–Dobruja Land [74],

whence may come the tourmaline currently occurring in exotic rocks [123,124] and as detrital grains in the Outer Carpathian flysch deposits [18]. The tourmalines from this source are also classified as schorl-dravite, with a fluorine content less than 0.1 apfu [18,110,123,124]. The crystalline rocks, in which dravite dominates over schorl, as in tourmaline separated from Albian sands and sandstones (Figure 10), are relatively scarce. These include pegmatites of the Szklary and Gogołów–Jordanów Massifs [35], granites and pegmatites in Tatra Mountains [35,125], mica schists of the Svratka Unit in the Czech Republic [34], quartz-sericite shales from Jegłowa in the eastern Sudetes [54] or some pegmatites [126] and marbles from the Bohemian Massif [60].

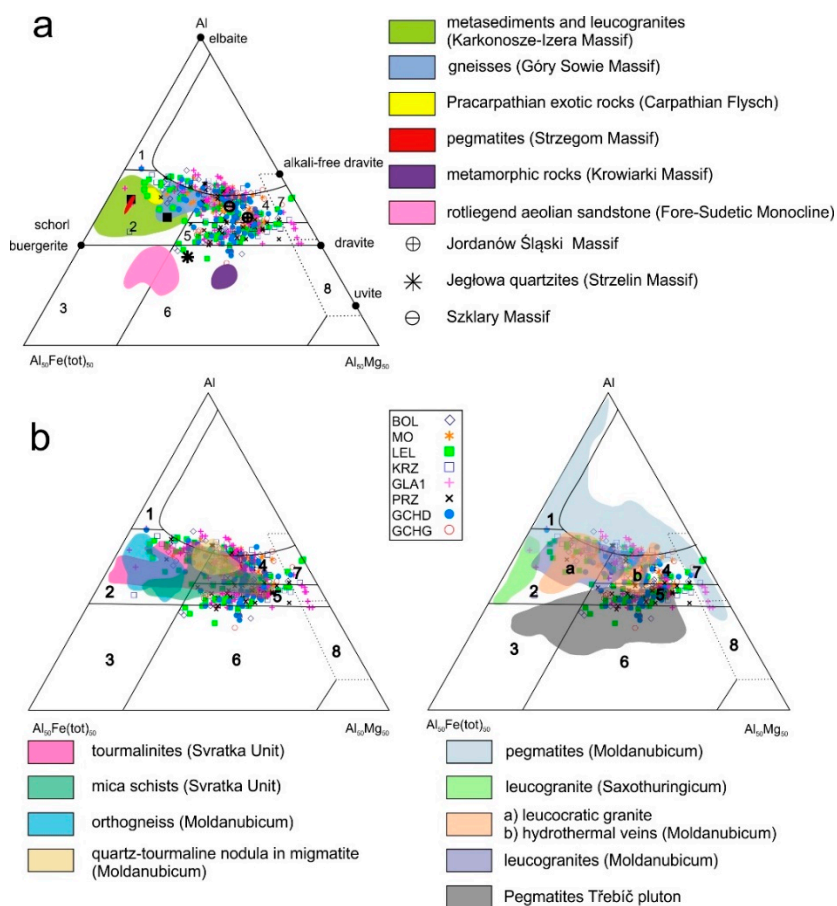


Figure 10. Comparison of detrital tourmalines from the study area plotted in Fe–Al–Mg ternary diagrams of Henry and Guidotti [69]. Coloured fields reflect the chemical composition of tourmalines from (a) different rock types and localities of Poland [35]; (b) different rock types and localities of Bohemian Massif [17,18,22,55,58,126–130]. Explanation for fields (1–8) the same as in Figure 8.

The potential source rock body had to be of considerable size, given the large volume and lateral extent of the Albian sands in the study area. However, some types of rocks despite of their relatively small volume size could contain high abundances of specific minerals (the so called high mineral fertility) [32,131,132]. Pegmatite thickness rarely exceeds a few meters [133,134]; nonetheless, pegmatites generally contain substantial amounts of tourmaline [35,68,133,135]. Pegmatite tourmaline compositions generally differ from ones studied in this paper (see Figure 8) and therefore, only a small portion of detrital tourmaline grains from Albian sands could have been derived from pegmatites. The marbles should also be excluded from further consideration, due to the low Ca contents in the tourmaline (Figure 6). The dravite dominant tourmaline assembly was also found in graphitic gneisses of the Velké and Malé Vrbno units, eastern part of the Bohemian Massif [57]. These crystals have a high-magnesium content and are from the dravite-uvite series (dravite 95–uvite 5). They are thought to be tourmalines originating from medium-grade metamorphosed metapelites and Ca-rich

metasediments. However, due to the very high Mg content (10–11 wt% MgO), they cannot be the main source of clastic material for samples from the study area (Table 3). The tourmalines from the Miechów Segment contain significantly less magnesium (on average around 5–8 wt% MgO) than tourmaline from the Vrbno Units (Table 3), ultimately eliminating the tourmalines from the Vrbno units as a major source of detrital material deposited in the Miechów area during the late Albian. The dravite dominant tourmaline from the Albian sands (Table 2) show strong similarity to tourmaline from the Jegłowa crystalline schists unit [35] and to the tourmaline described in rocks from the Svratka Unit [34] (Figure 10, Table 2). Both mentioned tectonostratigraphic units are in the eastern part of Bohemian Massif.

Some tourmaline grains in Lelów and Korzkiew (Figure 8) tend to concentrate in the field of Li-poor granitoids, aplites and pegmatites on the Henry and Guidotti [69] diagram. In most cases, excluding Mokresz and the Chełmo Mount, there is a distinct diagonal trend in previously mentioned diagrams (Figure 8). This might be caused by an influence of a different, additional source source. This trend is most visible in the most south-western part of the sampled area (Korzkiew, Głanów–Stroniczki, Przychody and Lelów). It is probable that most of the material was supplied by low- to medium-grade metamorphic rocks but some may have originated from felsic igneous massifs southwestern of the sampled area. The composition of tourmaline studied here is quite similar to that of tourmalines in gneisses of the Góry Sowie Block (northern part of Bohemian Massif), which point to this area as an additional source of detrital material for the Albian sands (Figure 10) [35].

The other adjacent source area, represented by the hypothetical HCMDL [74], and its extension towards the SE to the area now covered by the Outer Carpathian nappes (Figure 1), is very poorly documented for the mineral chemistry of tourmaline. Little information comes from the study of exotic rocks in the Outer Carpathian formations [35,123,124] and data from studies of heavy minerals in the Cretaceous, Paleogene and Neogene deposits, which currently form the Outer Carpathians [18]. A comparison of the available mineralogical data (Table 3) allows us to exclude a significant share of this source of clastic material. Tourmalines from S and SE of this source area are very rich in Fe and their composition places them on classification diagrams in the field of schorl. A similar composition is characteristic of tourmalines associated with granitoid intrusions currently occurring in Slovakia [136]. In these areas [136], only tourmalines occurring in metasomatic haloes around granitoid intrusions and in epigenetic quartz veins have a composition similar to dravite. Taking into account the size of the HCMDL sediment source area (Figure 1) and its potential denivelation above sea level in comparison to the Bohemian Massif, it can be inferred that the HCMDL should be excluded as a substantial source area.

The other two sources related to the crystalline basement of the European Platform (the Fennoscandian and Ukrainian Shields) probably had a small share in the delivery of clastic material to the Miechów area, mainly due to their considerable distance. Moreover, these areas are mostly built of gneisses and granitoids of different ages [137,138]; therefore, the mineral chemistry of the tourmaline should be close to schorl. These rocks are also rich in biotite and Ti-bearing magnetite, the components of which were not found in large amounts in the set of heavy minerals in the Albian sands from the vicinity of Miechów.

The compilation of information on the palaeogeography of extra-Carpathian area during the Albian and the compositions of our study tourmalines from Albian sands and sandstones indicate that the most probable sources for the Albian sands were rocks from the eastern metamorphic part of the Sudetes and the Bohemian Massif. The similar (almost the same) compositions of tourmalines, independent size and roundness of grains points to for the same source area during the entire Albian transgression.

Table 3. Comparison of examined tourmaline grains from the Miechów Segment with tourmaline from neighbouring source areas.

Locality	Poland						Bohemian Massif					
	This Paper	Carpathian Exotics [124]	Jęglowa Schists [35]	Gneisses, Góry Sowie [35]	Wołowa Góra [35]	Pegmatite, Tatry Mnt. [35]	Granite, Tatry Mnt. [125]	Dolomitic Marble [60]	Pegmatites, Moldanubicum [126]	Tourmalinite, Svratka Unit [34]	Schists, Svratka Unit [34]	Gneisses, Velke Vrbno [57]
Number of Analysis	(512)	(1)	(1)	(1)	(1)	(1)	(8)	(6)	(10)	(23)	(4)	(6)
SiO ₂	36.46	35.64	35.61	36.21	36.5	35.1	36.14	37.83	35.67	36.12	36.79	37.85
TiO ₂	0.64	0.26	0.56	0.77	0.27	0.53	0.26	0.07	0.64	0.87	0.68	0.47
B ₂ O ₃	10.67 *	7.8	10.37	10.61	10.58	10.4	10.49 *	10.82 *	10.44	10.56 *	10.66 *	10.81 *
Al ₂ O ₃	33.12	35.42	29.14	33.69	33.38	31.55	31.91	33.9	34.16	32.52	32.29	31.46
V ₂ O ₃	0.03	na	0.02	0.03	0.01	0.02	Na	na	na	0.04	0.06	0.14
Cr ₂ O ₃	0.03	na	0	0	0	0	Na	na	na	0	0	0.08
Fe ₂ O ₃	na	2.22	6.47	0.45	0.11	2.81	Na	na	0.69	na	na	na
FeO	6.78	11.2	6.7	6.96	6.62	7.56	10.64	1.68	9.43	10.6	8.2	0.39
MnO	0.03	0.12	0.13	0.06	0.02	0.07	0.06	na	0.1	0.03	0	0.03
ZnO	0.02	na	0.07	0.06	0.04	0.04	Na	na	na	na	na	0.01
MgO	6.34	2.1	5.52	5.5	6.3	5.67	5.12	9.49	3.41	4.31	6.08	11.02
CaO	0.42	0.84	0.72	0.61	0.54	0.76	0.3	0.83	0.3	0.3	0.31	1.07
Na ₂ O	1.97	1.89	1.63	1.42	1.77	1.73	2.09	1.89	1.69	2.13	2.26	2.23
K ₂ O	0.03	0.46	0.14	0.24	0.1	0.07	0.02	0.02	0.08	0.05	0.09	0.02
F	0	0.22	0.25	0.27	0.7	0.36	0.05	na	0.23	0.49	0.46	0.29
H ₂ O	3.66 *	2.02	3.14	3.37	3.18	3.41	3.59 *	3.31 *	2.98	3.28 *	3.23 *	3.58 *
Total	100.2	100.19	100.47	100.25	100.12	100.08	100.67	99.84	99.82	101.3	101.11	99.45

* calculated from stoichiometry.

The sea level was very low during the Early Cretaceous [1,2,139]. Significant areas of Europe were elevated above sea level [1] and were subject to intensive erosion (Figure 2) in the warm climate [140–142]. It is worth noting that the neo-Cimmerian tectonic movements phase during the latest Jurassic and earliest Cretaceous rejuvenated the old structures [1], such as the Bohemian Massif, as the source areas for clastic material. Subangular and angular detrital grains of minerals in Albian sands could probably have come directly from weathered and eroded crystalline rocks of the Bohemian Massif and Sudetes, and via rivers and streams could have been transported directly northward to the better peneplanised areas and to the epicontinental sea of an extra-Carpathian Poland.

It is possible that the detrital minerals in the Albian deposits could have been derived from sedimentary rocks older than the Albian. A terrestrial environment was present during most of the Early Cretaceous [73,143] and siliciclastic deposits (e.g., Permian, Lower Triassic, and pre-Albian Lower Cretaceous), covered the area of southern Poland. The sea transgressed roughly from the north [78,144] and encroaching onto the Miechów area could possibly have reworked older clastic sediments. The boundary between Upper Jurassic and Lower Cretaceous were not found in the outcrops studied here, although lower Cretaceous basal conglomerates have been reported in Miechów area by previous researchers [145,146]. The presence of these basal conglomerates in the Miechów Segment and the coexistence of material with different size fractions, roundness and degree of sorting may indicate a composite origin of the clastic material [72].

The maturity of the detrital material and the lack of the low-resistance detrital components, such as siltstones, limestones, clays, apatite, amphibole, pyroxene or Ca-rich plagioclase, in the Albian sediments may indicate either multiple processing and recycling stages of clastic material during which sediments underwent an aggressive chemical leaching during diagenesis and/or surface weathering conditions [31,147–150] or (less likely) a long transport of clastic components [151,152]. It is assumed that during the Early Cretaceous the Miechów area was covered by sand and gravel sediments with various thicknesses [5]. In the early stages of the Albian transgression, a central part of the present Miechów area was supposedly peninsular area covered by Lower Cretaceous siliciclastic detrital material [7,72,144,153]. It is highly possible that this area was the nearest land which supplied the detrital material to the Late Albian sea. These detrital grains must have undergone one or multiple sedimentary cycles, being transported from crystalline rock massifs onto a pre-Albian land in the central part of the Miechów Segment. This may explain the presence of well-rounded grains of detrital minerals in the study samples. On the other hand, the different degrees of roundness are a result of the detrital material being abraded over different times but generally in a short time from the geological point of view. It is worth noting that, in the study area, sandy beach environments were existing during the Albian [6]; thus, the well-rounded tourmaline grains could also be a result of an eolian abrasion. Eolian abrasion leading to well-rounded grains is a process much more effective than abrasion process occurring in the river and marine environment [31]. Although we cannot finally quantify the amount of recycled material in the studied Albian sand and sandstones, our data strongly suggest that the tourmaline grains were, either directly, or through recycling, derived from low- to medium-grade metamorphic rocks of the eastern Sudetes or/and the Bohemian Massif. It is worth noting that the assemblage of minerals found in various sedimentary rocks, i.e., in the Triassic [130] and Jurassic [17], are very similar in heavy mineral assemblages to the uppermost Lower Cretaceous sands and sandstones studied here. This indicates that the eastern metamorphic part of the Sudetes and the Bohemian Massif, as elevated land or large islands, were a major source of detrital material for almost all Mesozoic time.

6. Conclusions

The Albian sands from the Miechów Segment have a high sedimentological, mineralogical and petrographical maturity. The amount of accessory heavy minerals is less than 1% in predominantly quartz sand samples. The heavy minerals with a high resistance to chemical and physical weathering,

such as zircon, rutile, and tourmaline are dominant. The composition of the heavy mineral assemblage in analysed Albian sediments samples is similar from all examined localities of the Miechów Segment.

The chemically and physically resistant tourmalines reach up to 20% of the heavy mineral assemblage in the Miechów area. Nearly 70% of all tourmaline grains studied here are classified as dravite. The mineral chemistry of the detrital tourmaline is slightly diverse, but no significant chemical differences were found between the locations. The compositions of detrital tourmaline suggest a clear provenance from metamorphic rocks. Nearly all the studied grains can be classified as a low- to medium-grade metamorphic tourmaline, most probably crystallized up to amphibolite facies conditions. The most likely source rocks are crystalline Al-rich quartz muscovite schists and, to a lesser extent, muscovite rich gneisses; however, some of the detrital tourmalines may also have been derived from granites and pegmatites.

The Mg- and Ca-contents in tourmalines and the predominance of dravite over schorl in tourmaline from the Miechów area show the closest similarity to tourmalines from the crystalline schists from Jegłowa in the Sudetes, and to the tourmaline known in rocks from the Svatka Unit, eastern Bohemian Massif. This indicates that the most likely source area for Albian sands/sandstones seems to be the eastern, metamorphic part of the Bohemian Massif and the Sudetes.

The close similarity in the heavy mineral assemblages and the chemical composition of tourmaline grains in all the sampled localities imply similar conditions of sedimentation and the activity of the same sediment source area, as a main provenance source, during the entire Albian transgression in the Miechów area.

Supplementary Materials: The following are available online at <http://www.mdpi.com/2075-163X/10/10/0917/s1>. Table S1: Chemical composition of tourmaline from the Albian sands in the Miechów Synclinorium.

Author Contributions: Conceptualization, J.K.; methodology, J.K. and K.N.; software, J.K.; validation, J.K., K.N. and D.O.-N.; formal analysis, J.K. and D.O.-N.; investigation, J.K. and K.N.; resources, J.K.; data curation, J.K., K.N. and D.O.-N.; writing—original draft preparation, J.K.; writing—review and editing, J.K., D.O.-N., K.N.; visualization, J.K. and D.O.-N.; supervision, J.K.; project administration, J.K.; funding acquisition, J.K. and D.O.-N. All authors have read and agreed to the published version of the manuscript.

Funding: This work was supported by University of Warsaw (BOB-661-300/17) and Faculty of Geology, University of Warsaw (Cryo-SEM laboratory, National Multidisciplinary Laboratory of Functional Nanomaterials NanoFun project no. POIG.02.02.00-00-025/09; grants no: DSM 118210 and grant No. 501-D113-01-1130200).

Acknowledgments: The authors are greatly indebted to Jan Nowak, owner of the quarry near the Chełmo Mount for permission to conduct this scientific investigation. The warmest thanks are offered to Raymond Macdonald, for linguistic correction and helpful remarks; to Petras Jokubauskas and Beata Marciniak-Maliszewska for help with EPMA investigations.

Conflicts of Interest: The authors declare no conflict of interest.

References

1. Ziegler, P. *Shell Internationale Petroleum Maatschappij. Geological Atlas of Western and Central Europe*, 2nd ed.; Geological Society of London: London, UK, 1990.
2. Haq, B.U. Cretaceous eustasy revisited. *Glob. Planet. Chang.* **2014**, *113*, 44–58. [[CrossRef](#)]
3. Żelaźniewicz, A.; Aleksandrowski, P.; Buła, Z.; Karnkowski, P.H.; Konon, A.; Oszczytko, N.; Ślącza, A.; Żaba, J.; Żytko, K. *Regionalizacja Tektoniczna Polski*; Komitet Nauk Geologicznych PAN: Wrocław, Poland, 2011; ISBN 978-83-63377-01-4.
4. Marcinowski, R. The transgressive Cretaceous (Upper Albian through Turonian) deposits of the Polish Jura Chain. *Acta Geol. Pol.* **1974**, *24*, 117–220.
5. Hakenberg, M. Alb i cenoman w niecce miechowskiej. *Stud. Geol. Pol.* **1986**, *86*, 57–85.
6. Olszewska-Nejbert, D.; Kotowski, J.; Nejbert, K. Pylonichnus upsilon Frey, Curran and Pemberton, 1984 burrows and their environmental significance in transgressive Albian (Lower Cretaceous) sands of Głanów-Stroniczki, Cracow Upland, southern Poland. *Palaeogeogr. Palaeoclimatol. Palaeoecol.* **2020**, *538*. [[CrossRef](#)]
7. Jaskowiak-Schoeneichowa, M.; Krassowska, A. Paleomiąższości, litofacje i paleotektonika epikontynentalnej kredy górnej w Polsce. *Geol. Q.* **1988**, *32*, 177–198.

8. Poreba, E. Budowa geologiczna synkliny tomaszowskiej i jej baza surowcowa. In *Synklina Tomaszowska i Jej Znaczenie Surowcowe*; Mróz, J., Hammer, J., Poreba, E., Eds.; Akademia Górniczo-Hutnicza im. S. Staszica: Kraków, Poland, 1987; pp. 27–46.
9. Poreba, E. Litostratygrafia kredy dolnej w synklinie tomaszowskiej. In *Synklina Tomaszowska i Jej Znaczenie Surowcowe*; Mróz, J., Hammer, J., Poreba, E., Eds.; Akademia Górniczo-Hutnicza im. S. Staszica: Kraków, Poland, 1987; pp. 14–26.
10. Poreba, E.; Nieć, M.; Drożdż, S. Złoza piasków kwarcowych w niecce tomaszowskiej, stan i problemy ich dokumentowania. *Górnictwo Odkryw.* **2018**, *3*, 84–99.
11. Dadlez, R.; Marek, S.; Pokorski, J. *Geological Map of Poland without Cainozoic Deposit*; Ministerstwo Środowiska i Państwowy Instytut Geologiczny: Warsaw, Poland, 2000.
12. Ziegler, P. Evolution of the Arctic-North Atlantic and the Western Tethys: A visual presentation of a series of Paleogeographic-Paleotectonic maps. *AAPG Mem.* **1988**, *43*, 164–196.
13. Li, R.; Li, S.; Jin, F.; Wan, Y.; Zhang, S. Provenance of Carboniferous sedimentary rocks in the northern margin of Dabie Mountains, central China and the tectonic significance: Constraints from trace elements, mineral chemistry and SHRIMP dating of zircons. *Sediment. Geol.* **2004**, *166*, 245–264. [[CrossRef](#)]
14. Čopjaková, R.; Sulovský, P.; Paterson, B.A. Major and trace elements in pyrope-almandine garnets as sediment provenance indicators of the Lower Carboniferous Culm sediments, Drahaný Uplands, Bohemian Massif. *Lithos* **2005**, *82*, 51–70. [[CrossRef](#)]
15. Malone, J. The Rivers of Southeast Ireland and the Sands of the Irish Sea: Heavy Minerals Show that Proximity does not Always Predetermine Provenance. In *Heavy Minerals in Use, Developments in Sedimentology 58*; Mange, M., Wright, D.T., Eds.; Elsevier Science: Amsterdam, The Netherlands, 2007; pp. 547–568.
16. Morton, A.C.; Hallsworth, C. Stability of Detrital Heavy Minerals During Burial Diagenesis. In *Heavy Minerals in Use, Developments in Sedimentology*; Mange, M., Wright, D.T., Eds.; Elsevier Science: Amsterdam, The Netherlands, 2007; pp. 215–245. ISBN 9780444517531.
17. Salata, D. Heavy minerals as detritus provenance indicators for the Jurassic pre-Callovian palaeokarst infill from the Czatkowice Quarry (Kraków–Wieluń Upland, Poland). *Geol. Q.* **2013**, *57*, 537–550. [[CrossRef](#)]
18. Salata, D. Detrital tourmaline as an indicator of source rock lithology: An example from the Ropianka and Menilite formations (Skole Nappe, Polish Flysch Carpathians). *Geol. Q.* **2014**, *58*, 19–30. [[CrossRef](#)]
19. Dill, H.G.; Škoda, R. Provenance analysis of heavy minerals in beach sands (Falkland Islands/Islas Malvinas)—A view to mineral deposits and the geodynamics of the South Atlantic Ocean. *J. S. Am. Earth Sci.* **2017**, *78*, 17–37. [[CrossRef](#)]
20. Mange, M.A.; Morton, A.C. Geochemistry of heavy minerals. In *Heavy Minerals in Use, Developments in Sedimentology*; Mange, M.A., Wright, D.T., Eds.; Elsevier Science: Amsterdam, The Netherlands, 2007; pp. 345–391.
21. Preston, J.; Hartley, A.; Mange-Rajetzky, M.; Hole, M.; May, G.; Buck, S.; Vaughan, L. The Provenance of Triassic Continental Sandstones from the Beryl Field, Northern North Sea: Mineralogical, Geochemical, and Sedimentological Constraints. *J. Sediment. Res.* **2002**, *72*, 18–29. [[CrossRef](#)]
22. Biernacka, J. Provenance of Upper Cretaceous quartz-rich sandstones from the North Sudetic Synclinorium, SW Poland: Constraints from detrital tourmaline. *Geol. Q.* **2012**, *56*, 315–332. [[CrossRef](#)]
23. Harapińska-Depciuch, M. Materiały okruchowe w kredzie środkowej z osłony mezozoicznej Gór Świętokrzyskich. *Geol. Q.* **1957**, *1*, 449–461.
24. Harapińska-Depciuch, M. Petrografia osadów kredy górnej w północno-wschodniej części niżu polskiego. *Biul. Państwowego Inst. Geol.* **1972**, *261*, 171–257.
25. Ratajczak, T. Wyniki badań piasków synkliny tomaszowskiej w aspekcie możliwości wykorzystania ich przez przemysł szklarski. In *Synklina Tomaszowska i Jej Znaczenie Surowcowe*; Mróz, J., Hammer, J., Poreba, E., Eds.; Akademia Górniczo-Hutnicza im. S. Staszica: Kraków, Poland, 1987; pp. 47–58.
26. Łuszczkiewicz, A.; Kaczmarek, B. Ocena możliwości wydzielenia minerałów ciężkich z piasków szklarskich z rejonu Białej Góry. *Fizykochem. Probl. Miner.* **1992**, *25*, 123–132.
27. Kotowski, J.; Nejbert, K.; Olszewska-Nejbert, D. Chemistry and provenance of tourmaline from Albian sands of southern Poland. In Proceedings of the Joint 5th Central-European Mineralogical Conference and 7th Mineral Sciences in the Carpathians Conference, Banská Štiavnica, Slovakia, 26–30 June 2018; p. 54.

28. Hubert, J.F. A zircon-tourmaline-rutile maturity index and the interdependence of the composition of heavy mineral assemblages with the gross composition and texture of sandstones. *SEPM J. Sediment. Res.* **1962**, *32*, 440–450. [[CrossRef](#)]
29. Garzanti, E.; Andò, S. Plate Tectonics and Heavy Mineral Suites of Modern Sands. In *Heavy Minerals in Use, Developments in Sedimentology*; Mange, M.A., Wright, D.T., Eds.; Elsevier Science: Amsterdam, The Netherlands, 2007; pp. 741–763. ISBN 9780444517531.
30. Dinis, P.A.; Soares, A.F. Stable and ultrastable heavy minerals of alluvial to nearshore marine sediments from Central Portugal: Facies related trends. *Sediment. Geol.* **2007**, *201*, 1–20. [[CrossRef](#)]
31. Garzanti, E. The maturity myth in sedimentology and provenance analysis. *J. Sediment. Res.* **2017**, *87*. [[CrossRef](#)]
32. Garzanti, E.; Andò, S. Heavy minerals for junior woodchucks. *Minerals* **2019**, *9*, 148. [[CrossRef](#)]
33. Slack, J.F.; Palmer, M.R.; Stevens, B.P.J.; Barnes, R.G. Origin and significance of tourmaline-rich rocks in the Broken Hill district, Australia. *Econ. Geol.* **1993**, *88*, 505–541. [[CrossRef](#)]
34. Čopjaková, R.; Buriánek, D.; Škoda, R.; Houzar, S. Tourmalinites in the metamorphic complex of the Svratka Unit (Bohemian Massif): A study of compositional growth of tourmaline and genetic relations. *J. Geosci.* **2009**, *54*, 221–243. [[CrossRef](#)]
35. Pieczka, A. Studium mineralogiczne turmalinów Polski. *Pract. Mineral.* **1996**, *85*, 1–79.
36. Henry, D.J.; Novák, M.; Hawthorne, F.C.; Ertl, A.; Dutrow, B.L.; Uher, P.; Pezzotta, F. Nomenclature of the tourmaline-supergroup minerals. *Am. Mineral.* **2011**, *96*, 895–913. [[CrossRef](#)]
37. Janeczek, J. Typomorphic minerals of pegmatites from the Strzegom-Sobotka granitic massif. *Geol. Sudetica* **1985**, *20*, 1–82.
38. Roda-Robles, E.; Pesquera, A.; Velasco, F. Tourmaline in granitic pegmatites and their country rocks, Fregeneda area, Salamanca, Spain. *Can. Mineral.* **1995**, *33*, 835–848.
39. Černý, P.; London, D.; Novák, M. Granitic pegmatites as reflections of their sources. *Elements* **2012**, *8*, 289–294. [[CrossRef](#)]
40. Škoda, R.; Novák, M. Granitic pegmatites of the Třebíč syenite pluton, Moldanubian zone, Czech Republic; An example of NYF to mixed pegmatites related to the orogenic pluton. *Acta Mineral. Abstr. Ser. Szeged* **2012**, *7*, 126–127.
41. Gadas, P.; Novák, M.; Cempírek, J.; Buriánek, D.; Čopjaková, R.; Haifler, J.; Houzar, S.; Hreus, S.; Loun, J.; Kocáb, J.; et al. *Tourmalines of the Eastern Part of the Bohemian Massif*; Gadas, P., Novák, M., Eds.; Tigris: Zlín, Czech Republic, 2017; ISBN 978-80-7490-157-7.
42. Pichavant, M.; Manning, D. Petrogenesis of tourmaline granites and topaz granites; the contribution of experimental data. *Phys. Earth Planet. Inter.* **1984**, *35*, 31–50. [[CrossRef](#)]
43. Povondra, P.; Lang, M.; Pivec, E.; Ulrych, J. Tourmaline from the Příbyslavice peraluminous alkali-feldspar granite, Czech Republic. *J. Czech Geol. Soc.* **1998**, *43*, 3–8.
44. Buriánek, D.; Novák, M. Morphological and compositional evolution of tourmaline from nodular granite at Lavičky near Velké Meziříčí, Moldanubicum, Czech Republic. *J. Czech Geol. Soc.* **2004**, *49*, 81–90.
45. Maloney, J.S.; Nabelek, P.I.; Sirbescu, M.-L.C.H. Lithium and its isotopes in tourmaline as indicators of the crystallization process in the San Diego County pegmatites, California, USA. *Eur. J. Mineral.* **2008**, *20*, 905–916. [[CrossRef](#)]
46. Pieczka, A.; Ertl, A.; Gołębiewska, B.; Jeleń, P.; Kotowski, J.; Nejbort, K.; Stachowicz, M.; Giester, G. Crystal structure and Raman spectroscopic studies of OH stretching vibrations in Zn-rich fluor-elbaite Raman spectroscopic studies of OH stretching vibrations in Zn-rich fluor-ebaite. *Am. Mineral.* **2020**, in press. [[CrossRef](#)]
47. Ota, T.; Kobayashi, K.; Kunihiro, T.; Nakamura, E. Boron cycling by subducted lithosphere; insights from diamondiferous tourmaline from the Kokchetav ultrahigh-pressure metamorphic belt. *Geochim. Cosmochim. Acta* **2008**, *72*, 3531–3541. [[CrossRef](#)]
48. Lussier, A.; Ball, N.A.; Hawthorne, F.C.; Henry, D.J.; Shimizu, R.; Ogasawara, Y.; Ota, T. Maruyamaite, $K(MgAl_2)(Al_5Mg)Si_6O_{18}(BO_3)_3(OH)_3O$, a potassium-dominant tourmaline from the ultrahigh-pressure Kokchetav massif, northern Kazakhstan: Description and crystal structure. *Am. Mineral.* **2016**, *101*, 355–361. [[CrossRef](#)]
49. Žáček, V.; Frýda, J.; Petrov, A.; Hyršl, J. Tourmalines of the povondraite—(oxy)dravite series from the cap rock of meta-evaporite in Alto Chapare, Cochabamba, Bolivia. *J. Czech Geol. Soc.* **2000**, *45*, 3–12.

50. Henry, D.J.; Sun, H.; Slack, J.F.; Dutrow, B.L. Tourmaline in meta-evaporites and highly magnesian rocks: Perspectives from Namibian tourmalinites. *Eur. J. Mineral.* **2008**, *20*, 889–904. [[CrossRef](#)]
51. Majka, J.; Sek, M.P.; Mazur, S.; Gołębiowska, B.; Pieczka, A. Polymetamorphic evolution of pelites inferred from tourmaline zoning—The Rędziny hornfels case study at the eastern contact of the Karkonosze Granite, Sudetes, Poland. *Mineralogia* **2018**, *49*, 17–34. [[CrossRef](#)]
52. Grew, E.S.; Sandiford, M. A staurolite-talc assemblage in tourmaline-phlogopite-chlorite schist from northern Victoria Land, Antarctica, and its petrogenetic significance. *Contrib. Mineral. Petrol.* **1984**, *87*, 337–350. [[CrossRef](#)]
53. Trägårdh, J. Tourmaline-bearing chlorite- and cordierite-rich mica schists in the Bergslagen region, south-central Sweden—An example of progressive metamorphism of magnesium-enriched felsic volcanic rocks. *Geol. Föreningen i Stock. Förhandlingar* **1990**, *112*, 199–202. [[CrossRef](#)]
54. Pieczka, A.; Kraczk, J. X-ray and Mössbauer study of tourmaline from the quartz-sericite schist of Jegłowa (Lower Silesia). *Mineral. Pol.* **2000**, *31*, 3–11.
55. Buriánek, D.; Čopjaková, R. Tourmaline from the mica schist of the Svratka Crystalline complex. *Acta Mus. Morav. Sci. Geol.* **2008**, *93*, 61–79.
56. Žaba, J. Geneza oraz metamorficzna ewolucja gnejsów i granitoidów masywu izerskiego stogu, Sudety zachodnie. *Geol. Sudetica* **1984**, *19*, 89–190.
57. Losos, Z.; Selway, J.B. Tourmaline of dravite-uvite series in graphitic rocks of the Velké Vrbno Group (Silesicum, Czech Republic). *J. Czech Geol. Soc.* **1998**, *43*, 45–52.
58. Breiter, K.; Čopjaková, R.; Gabašová, A.; Škoda, R. Chemistry and mineralogy of orthogneisses in the northeastern part of the Moldanubicum. *J. Geol. Soc. Lond.* **2005**, *4*, 81–94. [[CrossRef](#)]
59. Hellingwerf, R.H.; Gatedal, K.; Gallagher, V.; Baker, J.H. Tourmaline in the central Swedish ore district. *Miner. Depos.* **1994**, *29*, 189–205. [[CrossRef](#)]
60. Bačík, P.; Uher, P.; Cempírek, J.; Vaculovič, T. Magnesian tourmalines from plagioclase-muscovite-scapolite metaevaporite layers in dolomite marble near Prosetín (Olešnice Unit, Moravicum, Czech Republic). *J. Geosci.* **2012**, *57*, 143–153. [[CrossRef](#)]
61. Pieczka, A.; Buniak, A.; Majka, J.; Harryson, H. Si-deficient foitite with [4]Al and [4]B from the ‘Ługi-1’ borehole, Southwestern Poland. *J. Geosci.* **2011**, *56*, 389–398. [[CrossRef](#)]
62. Henry, D.J.; Dutrow, B.L. Tourmaline at diagenetic to low-grade metamorphic conditions: Its petrologic applicability. *Lithos* **2012**, *154*, 16–32. [[CrossRef](#)]
63. Biernacka, J. Insight into diagenetic processes from authigenic tourmaline: An example from Carboniferous and Permian siliciclastic rocks of western Poland. *Sediment. Geol.* **2019**, *389*, 73–90. [[CrossRef](#)]
64. Foit, F.F.; Rosenberg, P.E. Coupled substitutions in the tourmaline group. *Contrib. Mineral. Petrol.* **1977**, *62*, 109–127. [[CrossRef](#)]
65. Lussier, A.J.; Hawthorne, F.C.; Herwig, S.; Abdu, Y.; Aguiar, P.M.; Michaelis, V.K.; Kroeker, S. Mushroom elbaite from the Kat Chay mine, Momeik, near Mogok, Myanmar: II. Zoning and crystal growth. *Mineral. Mag.* **2008**, *72*, 999–1010. [[CrossRef](#)]
66. Ertl, A.; Marschall, H.R.; Glester, G.; Henry, D.J.; Schertl, H.P.; Ntaflos, T.; Luvizotto, G.L.; Nasdala, L.; Tillmanns, E. Metamorphic ultrahigh-pressure tourmaline: Structure, chemistry, and correlations to P-T conditions. *Am. Mineral.* **2010**, *95*, 1–10. [[CrossRef](#)]
67. Novák, M.; Škoda, R.; Filip, J.; Macek, I.; Vaculovič, T. Compositional trends in tourmaline from intragranitic NYF pegmatites of the třebíč pluton, Czech Republic: An electron microprobe, mössbauer and LA-ICP-MS study. *Can. Mineral.* **2011**, *49*, 359–380. [[CrossRef](#)]
68. van Hinsberg, V.J.; Henry, D.J.; Marschall, H.R. Tourmaline: An ideal indicator of its host environment. *Can. Mineral.* **2011**, *49*, 1–16. [[CrossRef](#)]
69. Henry, D.J.; Guidotti, C.V. Tourmaline as a petrogenetic indicator mineral—An example from the staurolite-grade metapelites of NW Maine. *Am. Mineral.* **1985**, *70*, 1–15.
70. Morton, A.C.; Whitham, A.G.; Fanning, C.M. Provenance of Late Cretaceous to Paleocene submarine fan sandstones in the Norwegian Sea: Integration of heavy mineral, mineral chemical and zircon age data. *Sediment. Geol.* **2005**, *182*, 3–28. [[CrossRef](#)]
71. Bačík, P.; Uher, P.; Ertl, A.; Jonsson, E.; Nysten, P.; Kanický, V.; Vaculovič, T. Zoned ree-enriched dravite from a granitic pegmatite in Forshammar, Bergslagen Province, Sweden: An EMPA, XRD and LA-ICP-MS study. *Can. Mineral.* **2012**, *50*, 825–841. [[CrossRef](#)]

72. Hakenberg, M. Paleotektonika i paleogeografia północnej części niecki miechowskiej w albie i cenomanie. *Stud. Geol. Pol.* **1978**, *58*, 8–104.
73. Świdrowska, J.; Hakenberg, M.; Poluhtovič, B.; Seghedi, A.; Višňakov, I. Evolution of the Mesozoic basins on the south western edge of the East European Craton (Poland, Ukraine, Moldova, Romania). *Stud. Geol. Pol.* **2008**, *130*, 3–130.
74. Samsonowicz, J. Szkic geologiczny okolic Rachowa nad Wisłą oraz transgresje albu i cenomanu w bródzkie północno-europejskiej. *Spraw. Pol. Inst. Geol.* **1925**, *3*, 45–118.
75. Pasternak, S.I.; Gawrilishin, V.I.; Ginda, V.A.; Kotsyubinsky, S.P.; Senkovsky, Y. Stratigraphy and fauna of the Cretaceous deposits of the west of the Ukraine (without the Carpathians). *Nauk. Dumka Kiev.* **1968**, 1–272.
76. Pożaryski, W. *Budowa Geologiczna Polski, T. IV, Tektonika, cz. 1, Niż Polski*; Pożaryski, W., Ed.; Wydawnictwa Geologiczne: Warszawa, Poland, 1974.
77. Cieśliński, S. Alb i cenoman północnego obrzeżenia Gór Świętokrzyskich (stratygrafia na podstawie głowonogów). *Pract. Inst. Geol.* **1959**, *26*, 7–95.
78. Cieśliński, S. Początki transgresji górnokredowej w Polsce (bez Karpat i Śląska). *Geol. Q.* **1959**, *3*, 943–964.
79. Walaszczyk, I. Turonian through Santonian deposits of the Central Polish Uplands; their facies development, inoceramid paleontology and stratigraphy. *Acta Geol. Pol.* **1992**, *42*, 1–122.
80. Jurkowska, A. Inoceramid stratigraphy and depositional architecture of the Campanian and Maastrichtian of the Miechów Synclinorium (southern Poland). *Acta Geol. Pol.* **2016**, *66*, 59–84. [[CrossRef](#)]
81. Marcinowski, R. The Cretaceous transgressive deposits east of Czestochowa (Polish Jura Chain). *Acta Geol. Pol.* **1970**, *20*, 413–449.
82. Chlebowski, R.; Hakenberg, M.; Marcinowski, R. Albian ammonite fauna from the Chełmowa Mt near Przedbórz (central Poland). *Bull. L'academie Pol. Sci. Ser. Sci. Terre* **1977**, *25*, 91–97.
83. Marcinowski, R.; Wiedmann, J. The Albian ammonites of Poland. *Palaentologia Pol.* **1990**, *50*, 1–94.
84. Hakenberg, M. Alb i cenoman między Małogoszczem a Staniewicami w południowo-zachodnim obrzeżeniu Gór Świętokrzyskich. *Stud. Geol. Pol.* **1969**, *26*, 7–126.
85. Kutek, J.; Głazek, J. The Holy Cross area, central Poland, in the Alpine cycle. *Acta Geol. Pol.* **1972**, *22*, 603–653.
86. Matyszkiewicz, J. Microfacies, sedimentation and some aspects of diagenesis of Upper Jurassic sediments from the elevated part of the Northern peri-Tethyan shelf: A comparative study on the Lochen area (Schwäbische Alb) and the Cracow area (Cracow-Wieluń Upland, Poland). *Berl. Geowiss. Abh.* **1997**, *21*, 1–111.
87. Marcinowski, R.; Radwański, A. A unique habitat of endolithic biota: Hurricane-induced limestone rubble in an Albian sand-mass of the Cracow Upland, southern Poland. *Acta Geol. Pol.* **2009**, *59*, 505–521.
88. Severin, K.P. *Energy Dispersive Spectrometry of Common Rock Forming Minerals*; Springer: Amsterdam, The Netherlands, 2004; ISBN 1402028407.
89. Pouchou, L.L.; Pichoir, F. "PAP" (phi-rho-z) procedure for improved quantitative microanalysis. In *Microbeam Analysis*; Armstrong, J.T., Ed.; San Francisco Press: San Francisco, CA, USA, 1985; pp. 104–106.
90. Reed, S.J.B. *Electron Microprobe Analysis and Scanning Electron Microscopy in Geology*; Cambridge University Press: New York, NY, USA, 2005.
91. Henry, D.J.; Dutrow, B.L. Metamorphic tourmaline and its petrologic applications. In *Boron: Mineralogy, Petrology and Geochemistry*; Anovitz, L.M., Grew, E.S., Eds.; De Gruyter: Berlin, Germany, 1996; Volume 33, pp. 503–558.
92. Marcinowski, R.; Radwański, A. The Mid-Cretaceous transgression onto the Central Polish Uplands (marginal part of the Central European Basin). *Zitteliana* **1983**, *10*, 65–95.
93. Marcinowski, R.; Radwański, A. A biostratigraphic approach to the mid-Cretaceous transgressive sequence of the Central Polish Uplands. *Cretac. Res.* **1989**, *10*, 153–172. [[CrossRef](#)]
94. Pożaryski, W. Zarys stratygrafii i paleogeografii kredy na niżu polskim. *Pract. Inst. Geol.* **1960**, *30*, 377–440.
95. Moryc, W.; Waśniowska, J. Utwory neokomskie z Baszni koło Lubaczowa. *Ann. Soc. Geol. Pol.* **1965**, *35*, 55–70.
96. Henry, D.J.; Dutrow, B.L. Tourmaline in a low grade clastic metasedimentary rock: An example of the petrogenetic potential of tourmaline. *Contrib. Mineral. Petrol.* **1992**, *112*, 203–218. [[CrossRef](#)]
97. Rosenberg, P.E.; Foit, F.F. Magnesiofoitite from the uranium deposits of the Athabasca Basin, Saskatchewan, Canada. *Can. Mineral.* **2006**, *44*, 959–965. [[CrossRef](#)]

98. Williamson, B.J.; Spratt, J.; Adams, J.T.; Tindle, A.G.; Stanley, C.J. Geochemical constraints from zoned hydrothermal tourmalines on fluid evolution and Sn mineralization: An example from fault breccias at Roche, SW England. *J. Petrol.* **2000**, *41*, 1439–1453. [[CrossRef](#)]
99. Slack, J.F.; Trumbull, R.B. Tourmaline as a recorder of ore-forming processes. *Elements* **2011**, *7*, 321–326. [[CrossRef](#)]
100. Buriánek, D.; Dolníček, Z.; Novák, M. Textural and compositional evidence for a polyphase saturation of tourmaline in granitic rocks from the Třebíč Pluton (Bohemian Massif). *J. Geosci.* **2016**, *61*, 309–334. [[CrossRef](#)]
101. Codeço, M.S.; Weis, P.; Trumbull, R.B.; Van Hinsberg, V.; Pinto, F.; Lecumberri-Sanchez, P.; Schleicher, A.M. The imprint of hydrothermal fluids on trace-element contents in white mica and tourmaline from the Panasqueira W–Sn–Cu deposit, Portugal. *Miner. Depos.* **2020**. [[CrossRef](#)]
102. Marschall, H.R.; Korsakov, A.V.; Luvizotto, G.L.; Nasdala, L.; Ludwig, T. On the occurrence and boron isotopic composition of tourmaline in (ultra)high-pressure metamorphic rocks. *J. Geol. Soc. Lond.* **2009**, *166*, 811–823. [[CrossRef](#)]
103. Werding, G.; Schreyer, W. Experimental studies on borosilicates and selected borates. In *Boron: Mineralogy, Petrology and Geochemistry; Mineralogical Society of America, Reviews in Mineralogy*; Grew, E.S., Anovitz, L.M., Eds.; De Gruyter: Berlin, Germany, 2002; pp. 117–163.
104. Shimizu, R.; Ogasawara, Y. Diversity of potassium-bearing tourmalines in diamondiferous Kokchetav UHP metamorphic rocks: A geochemical recorder from peak to retrograde metamorphic stages. *J. Asian Earth Sci.* **2013**, *63*, 39–55. [[CrossRef](#)]
105. Thomson, J.A. A rare garnet-tourmaline-sillimanite-biotite-ilmenite-quartz assemblage from the granulite-facies region of south-central Massachusetts. *Am. Mineral.* **2006**, *91*, 1730–1738. [[CrossRef](#)]
106. van Hinsberg, V.J.; Schumacher, J.C.; Kearns, S.; Mason, P.R.D.; Franz, G. Hourglass sector zoning in metamorphic tourmaline and resultant major and trace-element fractionation. *Am. Mineral.* **2006**, *91*, 717–728. [[CrossRef](#)]
107. Keller, P.; Roda Robles, E.; Pesquera Pérez, A.; Fontan, F. Chemistry, paragenesis and significance of tourmaline in pegmatites of the Southern Tin Belt, central Namibia. *Chem. Geol.* **1999**, *158*, 203–225. [[CrossRef](#)]
108. Tindle, A.G.; Breaks, F.W.; Selway, J.B. Tourmaline in petalite-subtype granitic pegmatites: Evidence of fractionation and contamination from the Pakeagama lake and Separation lake areas of northwestern Ontario, Canada. *Can. Mineral.* **2002**, *40*, 753–788. [[CrossRef](#)]
109. Konzett, J.; Krenn, K.; Hauzenberger, C.; Whitehouse, M.; Hoinkes, G. High-pressure tourmaline formation and fluid activity in Fe-Ti-rich eclogites from the Kreuzeck Mountains, Eastern Alps, Austria. *J. Petrol.* **2012**, *53*, 99–125. [[CrossRef](#)]
110. Aubrecht, R.; Bačík, P.; Mikuš, T.; Bellová, S. Detritic tourmalines with complex zonation in the Cretaceous exotic flysches of the Western Carpathians: Where did they come from? *Lithos* **2020**, 105443. [[CrossRef](#)]
111. Hawthorne, F.C.; Ungaretti, L.; Oberti, R.; Caucia, F.; Callegari, A. The crystal chemistry of staurolite. II. Order-disorder and the monoclinic → orthorhombic phase transition. *Can. Mineral.* **1993**, *31*, 583–595.
112. Spear, F.S.; Kohn, M.J.; Cheney, J.T. P-T paths from anatectic pelites. *Contrib. Mineral. Petrol.* **1999**, *134*, 17–32. [[CrossRef](#)]
113. Althaus, E. The triple point andalusite–sillimanite–kyanite. An experimental and petrologic study. *Contrib. Mineral. Petrol.* **1967**, *16*, 29–44. [[CrossRef](#)]
114. Howie, R.A. Other Silicates. In *Encyclopedia of Geology*; Selley, R.C., Cocks, L.R.M., Plimer, I.R., Eds.; Elsevier Academic: Amsterdam, The Netherlands, 2005; pp. 561–567. ISBN 9780123693969.
115. Piccoli, P.M.; Candela, P.A. Apatite in Igneous Systems. *Rev. Mineral. Geochem.* **2002**, *48*, 255–292. [[CrossRef](#)]
116. Morton, A.C. Dissolution of apatite in North Sea Jurassic sandstones: Implications for the generation of secondary porosity. *Clay Miner.* **1986**, *21*, 711–733. [[CrossRef](#)]
117. Morton, A.C.; Hallsworth, C.R. Processes controlling the composition of heavy mineral assemblages in sandstones. *Sediment. Geol.* **1999**, *124*, 3–29. [[CrossRef](#)]
118. Bateman, R.M.; Catt, J.A. Provenance and palaeoenvironmental interpretation of superficial deposits, with particular reference to post-depositional modification of heavy mineral assemblages. In *Heavy Minerals in Use, Developments in Sedimentology*; Mange, M.A., Wright, D.T., Eds.; Elsevier Science: Amsterdam, The Netherlands, 2007; pp. 151–188. ISBN 9780444517531.

119. Garzanti, E.; Andò, S.; Vezzoli, G. Settling equivalence of detrital minerals and grain-size dependence of sediment composition. *Earth Planet. Sci. Lett.* **2008**, *273*, 138–151. [[CrossRef](#)]
120. Aleksandrowski, P.; Kryza, R.; Mazur, S.; Żaba, J. Kinematic data on major Variscan strike-slip faults and shear zones in the Polish Sudetes, northeast Bohemian Massif. *Geol. Mag.* **1997**, *134*, 727–739. [[CrossRef](#)]
121. Klomínský, J.; Jarchovský, T.; Rajpoot, G.S. *Atlas of Plutonic Rocks and Orthogneisses in the Bohemian Massif*; Czech Geological Survey: Prague, Czech Republic, 2010; ISBN 9788070757512.
122. Pieczka, A.; Szuszkiewicz, A.; Szełęg, E.; Nejbort, K.; Łodziński, M.; Ilnicki, S.; Turniak, K.; Banach, M.; Hołub, W.; Michałowski, P.; et al. (Fe,Mn)-(Ti,Sn)-(Nb,Ta) oxide assemblage in a little fractionated portion of a mixed (NYF + LCT) pegmatite from Piława Górna, the Sowie Mts. Block, SW Poland. *J. Geosci.* **2013**, *58*, 91–112. [[CrossRef](#)]
123. Tyniec, T. Pegmatyt turmalinowy z zachodnich Prakarpat. *Ann. Soc. Geol. Pol.* **1952**, *22*, 277–287.
124. Skoczylas-Ciszewska, K.; Tyniec, T. O pegmatycie turmalinowym z fliszu okolicy Żegociny. *Arch. Mineral.* **1955**, *18*, 187–210.
125. Gawęda, A.; Müller, A.; Stein, H.; Kadziołko-Gaweł, M.; Mikulski, S. Age and origin of the tourmaline-rich hydraulic breccias in the Tatra Granite, Western Carpathians. *J. Geosci.* **2013**, *58*, 133–148. [[CrossRef](#)]
126. Novák, M.; Povondra, P.; Selway, J.B. Schorl–oxy-schorl to dravite–oxy-dravite tourmaline from granitic pegmatites; examples from the Moldanubicum, Czech Republic. *Eur. J. Mineral.* **2004**, *16*, 323–333. [[CrossRef](#)]
127. Buriánek, D.; Novák, M. Tourmaline-bearing leucogranites from the Třebíč Pluton in the Moldanubicum. *GeoLines* **2003**, *16*, 155–156.
128. Słaby, E.; Kozłowski, A. Composition of tourmalines from tin-tungsten-bearing country rock of the Variscan Karkonosze granitoid—A record of the wall rock and hydrothermal fluid interaction. *Neues Jahrb. für Mineral. Abhandlungen* **2005**, *181*, 245–263. [[CrossRef](#)]
129. Bačík, P.; Uher, P.; Sýkora, M.; Lipka, J. Low-A1 tourmalines of the schorl–dravite–povondraite series in redeposited tourmalinites from the western Carpathians, Slovakia. *Can. Mineral.* **2008**, *46*, 1117–1129. [[CrossRef](#)]
130. Kowal-Linka, M.; Stawikowski, W. Garnet and tourmaline as provenance indicators of terrigenous material in epicontinental carbonates (Middle Triassic, S Poland). *Sediment. Geol.* **2013**, *291*, 27–47. [[CrossRef](#)]
131. Moecher, D.P.; Samson, S.D. Differential zircon fertility of source terranes and natural bias in the detrital zircon record: Implications for sedimentary provenance analysis. *Earth Planet. Sci. Lett.* **2006**, *247*, 252–266. [[CrossRef](#)]
132. Flowerdew, M.J.; Fleming, E.J.; Morton, A.C.; Frei, D.; Chew, D.M.; Daly, J.S. Assessing mineral fertility and bias in sedimentary provenance studies: Examples from the Barents Shelf. *Geol. Soc. Lond. Spec. Publ.* **2019**. [[CrossRef](#)]
133. Novák, M.; Kadlec, T.; Gadas, P. Geological position, mineral assemblages and contamination of granitic pegmatites in the Moldanubian Zone, Czech Republic; examples from the Vlastějovice region. *J. Geosci.* **2013**, *58*, 21–47. [[CrossRef](#)]
134. Szuszkiewicz, A.; Szełęg, E.; Pieczka, A.; Ilnicki, S.; Nejbort, K.; Turniak, K.; Banach, M.; Łodziński, M.; Różniak, R.; Michałowski, P. The Julianna pegmatite vein system at the Piława Górna Mine, Góry Sowie Block, SW Poland—Preliminary data on geology and descriptive mineralogy. *Geol. Q.* **2013**, *57*, 467–484. [[CrossRef](#)]
135. Pieczka, A.; Gołębiowska, B.; Jeleń, P.; Włodek, A.; Szełęg, E.; Szuszkiewicz, A. Towards Zn-dominant tourmaline: A case of Zn-rich fluor-elbaite and elbaite from the julianna system at Piława Górna, lower Silesia, SW Poland. *Minerals* **2018**, *8*, 126. [[CrossRef](#)]
136. Broska, I.; Petřík, I.; Uher, P. *Accessory Minerals of the Carpathian Granitic Rocks*; Slovenská Akadémia Ved, Bratislava: Bratislava, Slovakia, 2012.
137. Bogdanova, S.V.; Bingen, B.; Gorbatshev, R.; Kheraskova, T.N.; Kozlov, V.I.; Puchkov, V.N.; Volozh, Y.A. The East European Craton (Baltica) before and during the assembly of Rodinia. *Precambrian Res.* **2008**, *160*, 23–45. [[CrossRef](#)]
138. Shumlyansky, L.; Hawkesworth, C.; Billström, K.; Bogdanova, S.; Mytrokhyn, O.; Romer, R.; Dhuime, B.; Claesson, S.; Ernst, R.; Whitehouse, M.; et al. The origin of the Palaeoproterozoic AMCG complexes in the Ukrainian Shield: New U-Pb ages and Hf isotopes in zircon. *Precambrian Res.* **2017**, *292*. [[CrossRef](#)]
139. Ruffell, A. Sea-level events during the Early Cretaceous in Western Europe. *Cretac. Res.* **1991**, *12*, 527–551. [[CrossRef](#)]

140. Fenner, J. Middle and Late Albian geography, oceanography, and climate and the setting of the Kirchrode I and II borehole sites. *Palaeogeogr. Palaeoclimatol. Palaeoecol.* **2001**, *174*, 5–32. [[CrossRef](#)]
141. Heimhofer, U.; Adatte, T.; Hochuli, P.A.; Burla, S.; Weissert, H. Coastal sediments from the Algarve: Low-latitude climate archive for the Aptian-Albian. *Int. J. Earth Sci.* **2008**, *97*, 785–797. [[CrossRef](#)]
142. Huber, B.T.; MacLeod, K.G.; Watkins, D.K.; Coffin, M.F. The rise and fall of the Cretaceous Hot Greenhouse climate. *Glob. Planet. Change* **2018**, *167*, 1–23. [[CrossRef](#)]
143. Marek, S. Paleomiąższości, litofacje i paleotektonika epikontynentalnej kredy dolnej w Polsce. *Geol. Q.* **1988**, *32*, 157–176.
144. Cieśliński, S. Rozwój bruzdy duńsko-polskiej na obszarze świętokrzyskim w albie, cenomanie i turonie dolnym. *Biul. Państwowego Inst. Geol.* **1976**, *295*, 249–271.
145. Różycki, S.Z. Alb, cenoman i turon w okolicy stacji Złoty Potok (koło Koniecpola). *Spraw. Pol. Inst. Geol.* **1937**, *9*, 19–56.
146. Hakenberg, M.; Jurkiewicz, H.; Woiński, J. Profile kredy środkowej w północnej części niecki miechowskiej. *Geol. Q.* **1973**, *17*, 763–786.
147. Suttner, L.J.; Basu, A.; Mack, G.H. Climate and the origin of quartz arenites. *J. Sediment. Petrol.* **1981**, *51*, 1235–1246. [[CrossRef](#)]
148. Chandler, F.W. Quartz arenites: Review and interpretation. *Sediment. Geol.* **1988**, *58*, 105–126. [[CrossRef](#)]
149. Mehring, J.L.; McBride, E.F. Origin of modern quartzarenite beach sands in a temperate climate, Florida and Alabama, USA. *Sediment. Geol.* **2007**, *201*, 432–445. [[CrossRef](#)]
150. Garzanti, E.; Vermeesch, P.; Vezzoli, G.; Andò, S.; Botti, E.; Limonta, M.; Dinis, P.; Hahn, A.; Baudet, D.; De Grave, J.; et al. Congo River sand and the equatorial quartz factory. *Earth-Sci. Rev.* **2019**, *197*, 102918. [[CrossRef](#)]
151. Garzanti, E.; Resentini, A.; Andò, S.; Vezzoli, G.; Pereira, A.; Vermeesch, P. Physical controls on sand composition and relative durability of detrital minerals during ultra-long distance littoral and aeolian transport (Namibia and southern Angola). *Sedimentology* **2015**, *62*, 971–996. [[CrossRef](#)]
152. White, A.F.; Buss, H.L. Natural Weathering Rates of Silicate Minerals. In *Treatise on Geochemistry*, 2nd ed.; Holland, H.D., Turekian, K.K., Eds.; Elsevier Inc.: Amsterdam, The Netherlands, 2013; Volume 7, pp. 115–155. ISBN 9780080983004.
153. Hakenberg, M.; Świdrowska, J. Evolution of the Holy Cross segment of the Mid-Polish Trough during the Cretaceous. *Geol. Q.* **1998**, *42*, 239–262.

Publisher's Note: MDPI stays neutral with regard to jurisdictional claims in published maps and institutional affiliations.



© 2020 by the authors. Licensee MDPI, Basel, Switzerland. This article is an open access article distributed under the terms and conditions of the Creative Commons Attribution (CC BY) license (<http://creativecommons.org/licenses/by/4.0/>).